Vilnius University
Faculty of Physics
Laser Research Center

Augustė Grigaravičienė

INVESTIGATION OF ULTRASHORT PULSE GENERATION IN THE SHORT-WAVE INFRARED SPECTRAL REGION USING STIMULATED RAMAN SCATTERING

Master's Thesis

Laser Physics and Optical Technologies
program

Student	Augustė Grigaravičienė
Approved	2026 - 05 - 22
Academic supervisor	dr. Paulius Mackonis
Consultant	dr. Julius Vengelis
Director of Laser Research Center	dr. Dalia Kaškelytė

Vilnius 2026

Vilniaus universiteto
Fizikos fakulteto
Lazerinių tyrimų centras

Augustė Grigaravičienė

ULTRATRUMPŲJŲ IMPULSŲ GENERACIJOS TYRIMAS TRUMPABANGĖJE INFRARAUDONOJOJE SPEKTRO SRITYJE TAIKANT PRIVERSTINĘ RAMANO SKLAIDĄ

Magistro studijų baigiamasis darbas

Lazerinės fizikos ir optinių technologijų
studijų programa

Studentė	Augustė Grigaravičienė
Leista ginti	2026 - 05 - 22
Darbo vadovas	dr. Paulius Mackonis
Konsultantas	dr. Julius Vengelis
Centro direktorė	dr. Dalia Kaškelytė

Vilnius 2026

Table of contents

List of Abbreviations

AOPDF – acousto-optic programmable dispersive filter

FROG – frequency-resolved optical gating

GVD – group velocity dispersion

HC-PCF – hollow core photonic crystal fiber

HHG – high-harmonic generation

MPC – multi-pass cell

OPCPA – optical parametric chirped pulse amplification

SC – supercontinuum

SHG-FROG – second-harmonic generation frequency-resolved optical gating

SPM – self-phase modulation

SRA – stimulated Raman amplification

SRRS – stimulated rotational Raman scattering

SRS – stimulated Raman scattering

SWIR – short-wave infrared

Introduction

High-energy ultrashort pulses in the short-wave infrared (SWIR, 1.3–3 μm) spectral region have emerged as a major area of interest in both industrial and scientific fields. In semiconductor manufacturing, pulses with durations of a few picoseconds are used for the internal modification of silicon, which is transparent at SWIR wavelengths but exhibits strong nonlinear absorption at high intensity levels [1]. Additionally, the ability to generate femtosecond pulse durations in this wavelength range enables the study of high-field physics, including efficient high-harmonic [2] and terahertz generation [3].

Currently, there exist a number of established technologies for this spectral range. These include thulium (Tm^{3+}) and holmium (Ho^{3+}) doped fiber and solid-state lasers which provide direct emission around 2 μm, as well as optical parametric chirped pulse amplifier (OPCPA) systems which offer wide spectral tunability [4]. However, many of these systems suffer from significant technical trade-offs. For example, fiber lasers are generally restricted in terms of their ability to produce high peak powers due to parasitic nonlinearities and lower optical damage threshold. In contrast, high energy OPCPA systems require multiple stages and strict phase-matching conditions. Furthermore, obtaining temporal compression with respect to the original pump pulse is a major technological hurdle, requiring a large number of expensive and bulky external dispersive compressors [5], [6] that reduce the efficiency of the entire system and increase its physical size.

Stimulated Raman scattering (SRS) in pressurized molecular gases like hydrogen (H_2) can provide a scalable alternative for high-energy wavelength conversion. The gaseous medium provides high optical damage threshold and low group velocity dispersion (GVD) [7] compared to solid-state nonlinear crystals. As a result, it is possible to maintain relatively short pulse durations over long interaction lengths. Although SRS is well-established in terms of wavelength conversion when using steady-state regime, there exists a significant research gap in the high-power transient regime of SRS. Here the laser pulse duration is significantly shorter than the vibrational dephasing time (T_2) of the molecules [8]. Operating in the transient SRS regime introduces higher excitation threshold [9], lower conversion efficiency [10] and competition between different nonlinear processes [11]. To date, hydrogen-filled hollow-core photonic crystal fiber (HC-PCF) has been the primary tool for managing these effects, achieving quantum efficiencies near 50% [12]. However, HC-PCFs remain impractical for high-energy industrial applications due to their physical lengths (often exceeding 5 m) [13], fragility, and low energy ceilings, resulting in Stokes pulse energy of less than 20 μJ [12]. As a result, a transition toward bulk pressurized gas cell configurations appears necessary to achieve the scalability and energy-handling requirements for high-energy SWIR sources.

To overcome the inherent inefficiencies associated with the transient regime, the technique of stimulated Raman amplification (SRA) initiated by an external seed can be employed. Based on our prior successful implementation of SC seed in rotational SRA [14], we are now examining it for vibrational SRA. Additionally, another hypothesis explored in this study is that the vibrational coherence of hydrogen gas can be used as a dynamic gain medium. We therefore examined the relationship between high-gain Raman amplification and self-phase modulation (SPM) as it relates to achieving pulse compression directly within the conversion medium.

This work investigates transient stimulated vibrational Raman scattering in high-pressure hydrogen gas cell using supercontinuum seed. The aim of this thesis is to experimentally investigate this process with 1030 nm, 1.3 ps pump pulses to identify the conditions necessary to generate 1.8 μm, sub-picosecond pulses without additional pulse compression.

The following tasks were set during the study:

1. To investigate stimulated Raman scattering in the transient regime and identify the processes limiting the SRS conversion efficiency.
2. To employ supercontinuum seed for stimulated Raman amplification in order to enhance conversion efficiency.
3. To evaluate the vibrational Stokes pulse duration and spatial beam profile, and to determine the optimal conditions for generating a pulse with a smooth temporal envelope.
4. To evaluate the influence of hydrogen gas pressure on the Stokes pulse generation threshold and conversion efficiency.
5. To evaluate the potential for "self-compression" – where nonlinear effects and Raman gain dynamics produce Stokes pulses significantly shorter than the original pump.

1. Literature Overview

1.1. Applications of short-wave infrared ultrashort pulses

In recent years, there has been a growing demand for high-energy ultrashort pulses in the short-wave infrared (SWIR) spectral range. This wavelength range is of particular interest across both industrial and scientific fields. Radiation above 1.4 μm is frequently termed as “eye-safe” as it has strong absorption in the cornea and vitreous body, therefore, does not reach the sensitive retina. This physical property results in an increase in the maximum permissible exposure for the human eye by several orders of magnitude compared to 1 μm laser radiation. As such, SWIR sources are highly suitable for free-space optical communications and long-range LIDAR in open air environments [15].

A transformative application for SWIR lasers is the nonlinear processing of narrow-bandgap semiconductor materials, most notably silicon (Si) and germanium (Ge) [16], [17]. While silicon is opaque to standard 800 nm or 1030 nm radiation due to linear absorption, it becomes transparent in the SWIR range (beyond 1.1 μm). This transparency, combined with high peak intensities from ultrashort pulses, enables in-volume modification through multi-photon absorption [1]. This is critical for 3D optical data storage, and the fabrication of internal photonic structures or waveguides within silicon-on-insulator (SOI) platforms [18]. The optimal duration is considered to be 1 ps – 10 ps [19]; in this range, the peak intensity is high enough to trigger two-photon absorption (TPA), but not so high that it triggers Kerr effect before the light reaches the focal point. For a 100 fs pulse, self-focusing in silicon is triggered at energies as low as ~1 nJ. However, because the energy required for permanent structural modification in silicon exceeds these few-nanojoule levels, the optical Kerr effect and pre-focal plasma formation inevitably deplete the pulse energy prior to delivery at the target focus [1]. In contrast with conventional CPA systems generating Gaussian pulses, the typical asymmetry and steep front on Stokes pulses [20] generated by transient SRA processes in hydrogen could provide an advantage in the in-volume modification of silicon. The delivery of the maximum intensity at a time when no significant defocusing plasma has formed may prevent "plasma shielding" and spatial filamentation which would allow for higher precision 3D structuring throughout the volume of silicon.

From a fundamental science perspective, high-energy femtosecond SWIR pulses serve as driving sources for high-harmonic generation (HHG). According to the λ^2 scaling law of the ponderomotive energy ($U_p \propto I\lambda^2$), it is possible to generate higher photon energies by going from a 1 μm to a 2 μm laser source. This extends the harmonic cut-off into the "water window" (280-530 eV) enabling soft X-ray imaging of biological samples in their native state [2]. Additionally, these pulses can be employed as driving sources for high-field terahertz (THz) generation in organic crystals, where the SWIR pump avoids the multi-photon absorption limits found with NIR pumps [3].

1.2. Ultrashort SWIR laser sources

The pursuit of high-energy, ultrafast SWIR sources has led to the development of several distinct laser architectures, yet each one has its own set of limitations that restrict further scaling. Rare-earth-doped fiber lasers (Fig. 1), primarily those utilizing Thulium (Tm^{3+}) and Holmium (Ho^{3+}) ions, have emerged as the leaders in average power scaling. Recent milestones in spectral beam combining have pushed these systems toward the 2 kW average power regime [21]. However, for applications requiring femtosecond pulses, the energy available from fiber lasers is limited μJ-level due to the high peak intensity confined within the small core area of the fiber. This leads to the early onset of the undesirable nonlinear effects including transverse mode instability and stimulated Brillouin scattering (SBS), that degrade the beam profile and limit the extractable energy. Furthermore, managing thermal loads at fiber splice points and implementing complex chirped-pulse amplification (CPA) schemes to prevent fiber damage remain significant barriers to achieving millijoule-level femtosecond pulse energies using compact laser designs [22] (Fig. 2a, b).

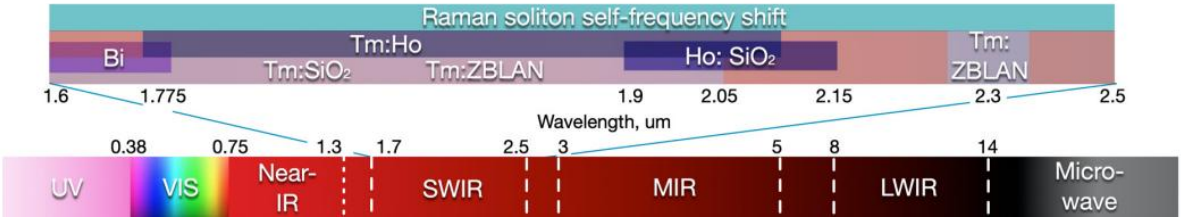

Fig. 1. SWIR wavelength range and possible fiber-based laser mediums [23].

Alternatively, bulk solid-state and thin-disk lasers based on Holmium-doped crystals such as Ho:YAG or Ho:YLF can provide the high pulse energies required for scientific and industrial processing [24], [25]. Unlike fibers, these systems can handle high peak powers in free-space geometry. However, Ho-doped media present unique integration challenges, most notably the requirement for non-standard, in-band pumping (typically at 1.908 μm). This necessitates secondary laser sources, such as Thulium-fiber lasers which increase system footprint and cost (Fig. 2c). Furthermore, these systems are fundamentally limited by the quasi-three-level transition of the Ho ion, which involves a thermally populated lower laser level. At room temperature, this results in significant reabsorption losses and high lasing thresholds, necessitating complex and costly cryogenic cooling systems [26] to achieve high efficiency and mitigate thermal lensing.

While thin-disk geometry improves heat dissipation by allowing one-dimensional heat flow, it introduces a conflict between the high inversion levels required to compensate for the limited disk thickness and the resulting increase in non-radiative losses, such as excited-state absorption and up-conversion [27]. To overcome the low single-pass absorption associated with such thin media, highly complex multi-pass pumping schemes are required. These schemes significantly increase the mechanical complexity and alignment sensitivity of the laser resonator. Due to these cumulative

challenges, 2 µm thin-disk technology remains in an earlier developmental stage compared to its established 1 µm counterparts.

Table 1. Different 2 µm lasers and their parameters. MOPA – master oscillator power amplifier, osc – oscillator, amp – amplifier.

Laser type	Gain medium	Pulse duration, ps	Pulse energy	Repetition rate	Ref.
Fiber	Tm/Ho:Fiber	0.4 – 0.6	1 – 50 nJ	10 – 100 MHz	[28]
Fiber (MOPA)	Tm:Fiber	0.5 – 2	10 – 500 µJ	0.1 – 1 MHz	[29]
Bulk (osc)	Ho:YAG/YLF	0.3 – 2	1 – 5 µJ	10 – 80 MHz	[30]
Bulk (amp)	Ho:YAG/YLF	2 – 15	50 – 260 mJ	0.1 – 1 kHz	[31]
Thin-disk (osc)	Ho:YAG	0.2 – 1.2	2 – 10 µJ	20 – 20 MHz	[32]
Thin-disk (amp)	Ho:YAG	Mostly CW	Average power 50 W		[27]

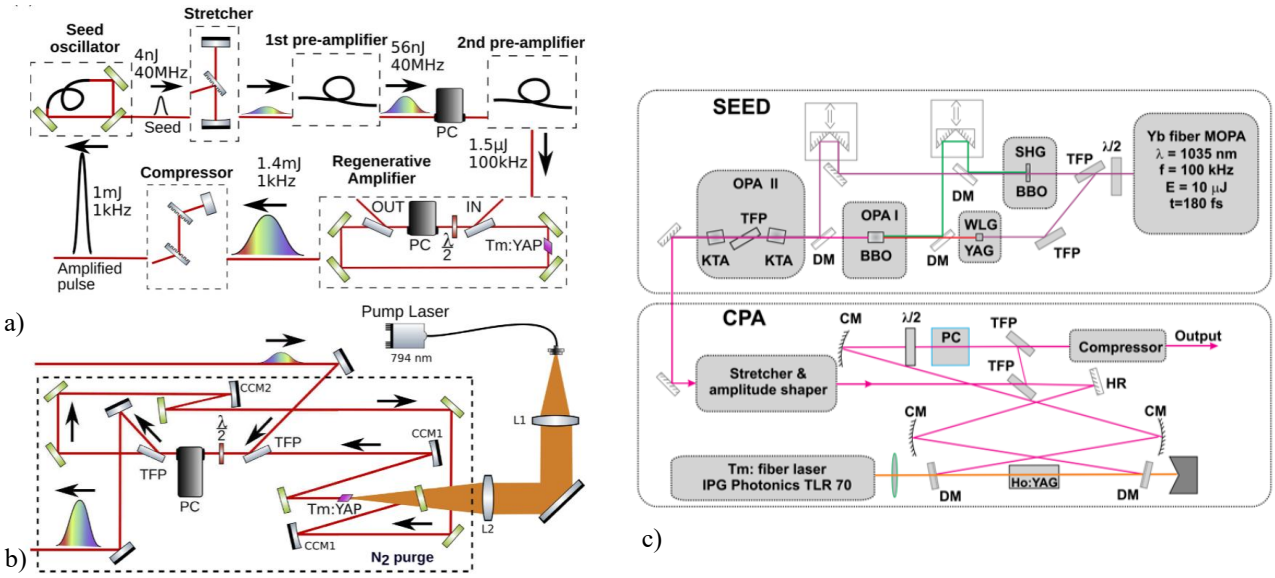

Fig. 2. Examples of high-energy ultrashort 2 µm lasers. Schematic diagram of a) the Tm laser system and b) detailed 25-pass regenerative amplifier; ouput parameters: 1 mJ, 1 kHz, 265 fs [33]. c) Layout of the Yb-fiber MOPA pumped OPA seed source and Ho:YAG CPA system (22-pass regenerative amplifier); output parameters: 3 mJ (before compression), 5 kHz, 530 fs [30].

To obtain the shortest pulse duration, the finite gain bandwidth of rare-earth-doped media can be overcome using nonlinear post-compression. Although thulium-doped fiber lasers support pulses down to ~200 fs [34], and holmium-doped solid-state lasers are generally limited to 500 fs [24], both of these pulse durations are still an order of magnitude too long to drive attosecond physics directly [35]. Therefore, nonlinear pulse compression methods are employed, e.g., self-phase modulation induced spectral broadening in gas-filled multi-pass cells (MPC) [5] or hollow-core fibers [6]. Researchers have successfully demonstrated pulse compression down to 10.2 fs (1.5 optical cycles) by filling a capillary with a noble gas and pumping it with a high-energy 2 µm source [36].

An alternative method for generating the high peak power, few cycle SWIR pulses is optical parametric chirped pulse amplification (OPCPA) systems that have been shown to be an advanced

state-of-the-art [37]. OPCPA systems transfer energy from a narrowband, high-energy pump to a broadband, low energy seed within a nonlinear crystal. It provides pulse durations as short as three optical cycles [38], and offers wide wavelength tunability. The seed sources used in most OPCPA systems are generated using Ti:sapphire oscillators coupled with difference frequency generation (DFG). In contrast, Ytterbium-driven front-ends, while offering better power scalability, present greater architectural complexity, typically necessitating supercontinuum generation and secondary OPA stages to reach the desired seed wavelengths. Despite its high performance, OPCPA requires complex multi-stage amplification and compression configurations that increase system size and operational cost. Moreover, the performance of OPCPA systems is strongly dependent upon maintaining temporal synchronization between the pump and signal pulses at sub-picosecond levels to ensure stable parametric gain [39]. Additionally, average power scaling is also limited due to residual absorption and optical damage threshold inherent to the nonlinear crystals. High average power operation of these crystals results in thermal lensing effects that distort the wavefront and limit long-term system stability. The cumulative challenges associated with current technologies emphasize the necessity of developing simplified and scalable frequency conversion architectures.

1.3. SRS for SWIR spectral range

An alternative solution for reaching the SWIR spectral region is stimulated Raman scattering (SRS) in compressed molecular gas. In comparison to solid-state Raman crystals, whose thermal conductivity is constrained to a specific temperature value and that have a rigid laser induced damage threshold, gaseous media like pressurized hydrogen (H_2), nitrogen (N_2), or methane (CH_4) can be considered as "self-healing", and thus allow for circulation to mitigate thermal effects within high average power systems [40]. The vibrational Raman shift in H_2 is particularly significant (4155 cm^{-1}), this represents a great opportunity to make a large spectral leap (from the standard 1030 nm Yb-doped laser emission to the 1.8 μm range) in a single Raman conversion step, with quantum efficiencies theoretically reaching up to 57 %. Furthermore, the interaction strength can be dynamically tuned via adjustment of the gas pressure, and therefore, the nonlinear gain can be optimized precisely [14].

However, as laser technology evolves towards shorter pulse durations, the SRS process enters the transient regime where the pump pulse duration (τ_p) becomes significantly shorter than the molecular dephasing time (T_2), which for hydrogen at high pressures is typically in the range of several hundred picoseconds. Under these conditions, the coherence of the medium cannot follow the rapid intensity fluctuations of the pump pulse [8], so the Raman gain will depend on the integrated energy of the pump pulse instead of the instantaneous pump intensity. As a result, substantial increase in the Raman threshold values is observed, along with a decrease in the maximum achievable

conversion efficiency in respect to what can be obtained under steady-state conditions [9]. Moreover, besides SRS, other nonlinear effects occur simultaneously during high intensity ultrashort pulse excitation. For example, supercontinuum generation, self-focusing and self-phase modulation may consume part of the pump energy either completely depleting it, or deviating into undesired anti-Stokes components [11], [41]. Therefore, it is critical to manage these effects for achieving an efficient coherent Stokes generation with good beam quality and smooth pulse envelope.

In order to overcome some of these issues, researchers have used hydrogen-filled hollow-core photonic crystal fibers. These fibers take advantage of very long interaction lengths and high intensities (Fig. 3.) and achieve quantum efficiencies close to 50% even in transient SRS regime with 300 fs pump pulse duration [12]. Nevertheless, HC-PCF systems remain largely limited to laboratory demonstrations due to mechanical fragility, high costs, size constraints (lengths are often exceeding 5 m) [13] and low energies (the Stokes output is typically lower than 20 μJ [12].

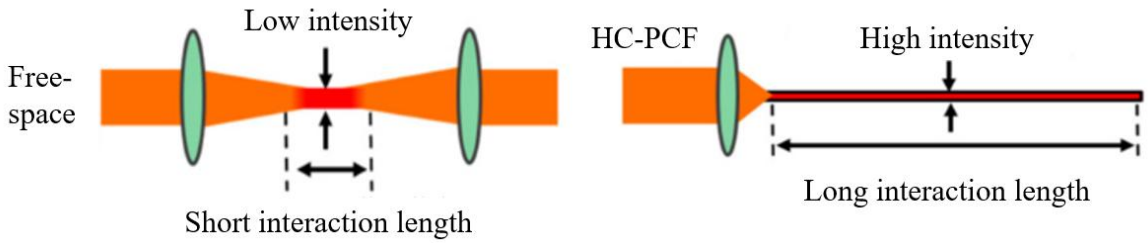

Fig. 3. Simplified schematic diagram of laser radiation and gas interaction in a) conventional Raman gas lasers and b) hollow-core photonic crystal fiber Raman gas lasers. [42].

A more scalable alternative investigated in this work is seeded stimulated Raman amplification (SRA). Seeding the Raman process at the Stokes wavelength with an external seed light allows the Raman scattering to start from deterministic condition instead from quantum noise. In previous studies performed in our laboratory it was demonstrated that by employing a supercontinuum as a seed source for Raman scattering, the SRS threshold decreases, energy stability is enhanced, and competing nonlinearities are suppressed [14], [43]. Up-to-date, high efficiency Raman conversion in the transient regime is realized mainly exploiting H_2-filled HC-PCFs. In contrast, transient SRA in compressed hydrogen cells has not been as extensively studied. Although, cell geometry offers an evident advantage with respect to simple structure and higher compatibility with high-energy, picosecond, 1 μm-class pump sources, it is however required that competing nonlinear effects are managed with particular care in the transient regime. Therefore, this work investigates the realization of SRA in a high-pressure H_2 gas cell, aiming for the efficient generation of sub-ps radiation at 1.8 μm.

2. Theory

2.1. Stimulated Raman Scattering

Spontaneous Raman scattering was first experimentally observed in 1928 by C. V. Raman and K. S. Krishnan [44]. It is characterized as an inelastic, non-coherent scattering process arising from the interactions of monochromatic light with matter. This interaction induces a spectral shift of the scattered light, called the Raman shift given by the relation:

$$\omega_R = \omega_p - \omega_s. \quad (1)$$

The Raman shift represents the difference in energy between the incident pump frequency (ω_p) and the scattered frequency (ω_s). There are two distinct regimes: Stokes and anti-Stokes. Stokes scattering corresponds to the case when the scattered photons possess a lower frequency (longer wavelength) than the incident light ($\omega_p - \omega_R$); conversely, anti-Stokes scattering corresponds to the case when the scattered photons have higher frequency (shorter wavelength) than the incident light ($\omega_p + \omega_R$).

The cause of spontaneous Raman scattering is microscopically rooted in the thermal or quantum mechanical induced fluctuations within the illuminated medium. Due to the relatively small cross-section of scattering (approximately ~10^{-6} cm^{-1} per unit volume in solids) the process is inherently inefficient. Only a fraction (roughly 10^{-6}) of the incident pump radiation is converted into Stokes radiation over 1 cm of propagation length. However, high-intensity laser sources allow for the condition to be met such that the system transitions into the stimulated Raman scattering regime, which was first reported by E. J. Woodbury's group using ruby laser in 1962 [45]. In SRS, the material interacts simultaneously with photons of two frequencies, ω_p and ω_s. While the initial Stokes photon is typically generated via spontaneous Raman scattering, the stimulated process results in the emission of additional ω_s photons which are coherent with the incident field. Therefore, the conversion efficiencies can reach several tens of percent [46].

When the Stokes pulse is being amplified, the gain will initially follow an exponential curve as it approaches saturation due to pump pulse depletion. Once a high conversion efficiency has been obtained, the primary Stokes wave acts as a secondary pump source $\omega_s - \omega_R = \omega_p - 2\omega_R$ enabling the generation of multiple order Stokes components. For example, after the first-order Stokes wave has grown out of quantum noise and is amplified within the pump field until saturation is reached and most of the pump has been depleted, this wave acts as the pump for generating a second-order Stokes component. Additionally, under certain phase-matching conditions, anti-Stokes radiation may be generated in a conical emission pattern. This specific process is governed by the third-order nonlinear susceptibility of the medium, creating a nonlinear polarization that oscillates at the frequency equal

to $\omega_a = \omega_p + \omega_p - \omega_s = \omega_p + \omega_R$, a mechanism fundamentally equivalent to four-wave mixing (FWM) [47].

2.2. Transient Stimulated Raman Scattering

The amplification of Stokes radiation within the Stimulated Raman Scattering (SRS) framework follows an exponential growth model, defined by the total gain increment G_{SS} and the Raman gain coefficient g_R. The temporal evolution of this process is intrinsically linked to the dephasing time (T_2) of the medium's vibrational modes – when using hydrogen with 3 MPa pressure, this parameter is around 250 ps [48].

The interaction is classified into two temporal domains based on the relationship between the pump pulse duration (τ_p) and the molecular relaxation dynamics. In the steady-state regime ($\tau_p > G_{SS}T_2$), the gain scales linearly with the incident pump intensity and the interaction length:

$$G_{ss} = g_R I_p l. \tag{2}$$

A distinctive feature of this regime is the observed spectral narrowing of the Stokes signal, a direct consequence of the preferential amplification at the peak of the Raman gain profile [49].

As pulse durations decrease into the picosecond or femtosecond range ($\tau_p < G_{SS}T_2$), the system enters the transient regime. Here, the gain G_T follows a sub-linear (square-root) dependence on the steady-state parameters:

$$G_T = \sqrt{4G_{SS}\frac{\tau_p}{T_2}}, \tag{3}$$

where $T_2 = 1/\pi c \Delta\omega_R$, $\Delta\omega_R$ – spontaneous Raman scattering spectral width.

While the transient regime is characterized by a diminished conversion efficiency and a higher operational threshold [50], it offers distinct advantages for pulse manipulation. The transient regime is often accompanied by complex nonlinear phenomena, including substantial spectral broadening via self-phase modulation [51] and competition with parasitic effects such as multiphoton absorption, self-focusing and supercontinuum generation [11].

2.3. Nonlinear effects

In high-intensity regimes, the optical response of a medium becomes nonlinearly proportional to the incident electric field. In centrosymmetric gases like hydrogen, third-order nonlinearities ($\chi^{(3)}$) dominate, primarily through the optical Kerr effect. This effect induces an intensity-dependent refractive index ($n = n_0 + n_2$, where n_0 and n_2 are the linear and nonlinear refractive indices of the media), which triggers self-action phenomena such as self-focusing and self-phase modulation (SPM). Self-focusing occurs if the pump peak power exceeds a critical power value:

$$P_{cr} = \frac{0.61^2\pi\lambda^2}{8n_0n_2}, \tag{4}$$

causing the medium to act as a converging lens [47]. Simultaneously, SPM causes the creation of new frequency components by modulating the phase of the pulse in time, leading to significant spectral broadening or even supercontinuum generation.

In the transient SRS regime, these nonlinear processes compete with Raman scattering for the energy of the pump pulse. While SPM expands the available bandwidth, it can simultaneously decrease the efficiency of stimulated Raman scattering. In high-intensity systems, managing this competition is essential to ensure that the pump pulse energy is efficiently channeled into the Stokes pulse rather than being lost to parasitic nonlinear effects. However, finding the balance between SPM and SRS could potentially allow to generate Stokes pulse with short duration while still maintaining sufficiently high efficiency.

2.4. Stimulated Raman amplification

The development of stimulated Raman scattering schemes started with nanosecond-scale pulses and gaseous media, which were favored for their large frequency shifts and high optical damage thresholds. However, when switching to ultrashort pulses, in the picosecond and femtosecond regime, the interaction moved from steady-state into the transient regime, which is defined by the condition where the pump pulse duration is shorter than the vibrational dephasing time (T_2) of the Raman-active molecules. In this regime, the process is often accompanied by significant spectral broadening and pulse compression. One of the main challenges associated with operating in the transient regime is the competition between SRS and the optical Kerr effect, which can degrade conversion efficiency and beam quality.

To mitigate this competition, the concept of chirped pulse Raman amplification was developed. It was demonstrated in 1994 [52] that using chirped pump pulses reduces the impact of self-focusing and allows for the generation of Stokes pulses as short as 85 fs. Temporally stretching the pump pulse also enables the use of waveguides with long interaction lengths, such as hollow-core fibers. For instance, in 2020 [53], a deuterium-filled HCF was used to demonstrate efficient conversion from 10 ps chirped pump pulses into 920 fs Stokes pulses at 2.68 μm.

Due to generally low energy conversion efficiency in a single stage of transient SRS, multi-stage architectures have become common. While gaseous media like hydrogen can achieve high conversion efficiency using 1 ps pulses, they are often limited by thermal lensing at high repetition rates (e.g., >1 kHz) [54]. Solid-state crystals, such as $Ba(NO_3)_2$ or KGW, offer superior thermal conductivities and therefore are more suitable for high average power operation. It was shown that a two-stage amplifier using barium nitrate could successfully amplify 200 ps chirped pulses, which were subsequently compressed to 100 fs while maintaining the phase of the pump [55].

The stability and quality of the Stokes output can be significantly improved by replacing the initial Raman generator with supercontinuum seed. It was demonstrated that seeding a hydrogen-based Raman amplifier with a supercontinuum significantly improved both the energy stability and spectral control [56]. This approach was further investigated, and it was found that the use of compressed versus a chirped pump pulse in KGW crystals drastically affects the resulting Stokes output [57]. Specifically, transform-limited pump pulse led to a five-fold increase in spectral width compared to a chirped pump pulse, due to increased phase modulation. Previous research in our laboratory has also shown that using a supercontinuum seed can reduce the rotational SRS threshold four-fold, while increasing conversion efficiency threefold in pressurized hydrogen gas [58]. Seeded stimulated Raman amplification represents one of the most promising methods for efficiently extending the range of ultrashort lasers into the SWIR region.

3. Experimental layout

The pump source used for the stimulated Raman scattering (SRS) experiments was developed during the first coursework (based on previous studies [59]). The Yb:YAG/Yb:LuAG chirped-pulse amplifier generates pulses at a 100 Hz repetition rate with an energy of 10 mJ, a spectral bandwidth of 1.6 nm (FWHM), and a central wavelength of 1030 nm. These pulses were compressed to a 1.3 ps duration using a diffraction grating pulse compressor. An attenuator, consisting of a half-wave plate (λ/2) and a thin-film polarizer (TFP), was used to adjust the pump pulse energy. The pump beam diameter is 2 mm (at the $1/e^2$ level), and the maximum energy was selected to prevent optical damage to the gas cell windows. The optical layout for the SRS excitation is shown in Fig. 4.

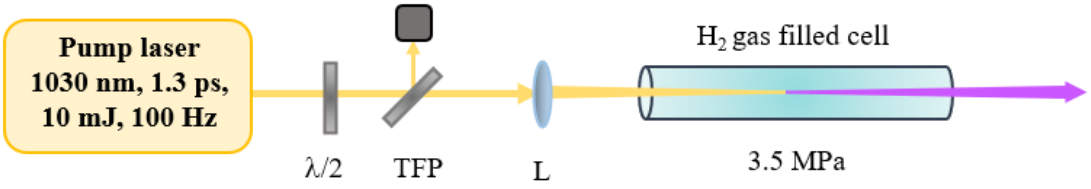

Fig. 4. Experimental layout of the excitation of SRS in compressed hydrogen gas. λ/2 – half-wave retardation plate, TFP – 45° thin film polarizer, L – focusing lens.

The experimental layout for stimulated Raman amplification (SRA) is illustrated in Fig. 5. A supercontinuum generated in a 130 mm long YAG crystal rod (with spectral broadening extending up to 2.5 μm) serves as the seed source.

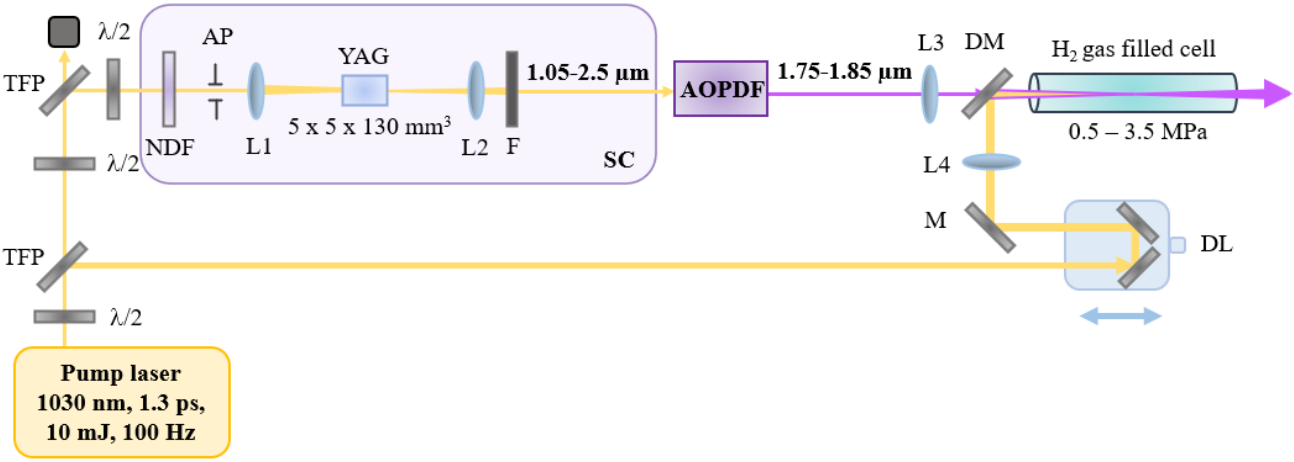

Fig. 5. Experimental layout of a stimulated Raman amplification with a seed signal. λ/2 – half-wave retardation plates, TFP – 45° thin film polarizers, NDF – neutral density filter, AP – aperture, L1, 2, 3, 4 – focusing lenses, F – interference filter, AOPDF – acousto-optic programmable dispersive filter, DM – dichroic mirror, M – 45° mirror, DL – delay line.

The supercontinuum radiation is collimated by an achromatic lens and directed into an acousto-optic programmable dispersive filter (AOPDF) (Dazzler WB45-1450-3000, Fastlite, France).

The AOPDF is used to select the seed's central wavelength to match the vibrational Stokes shift and spectrally filter the bandwidth to 100 nm (FWHM) in order to prevent unintended seeding of rotational Stokes components. Additionally, the second- and third-order dispersion are adjusted to compensate for the dispersion accumulated in the YAG rod and the AOPDF crystal, ensuring the generation of transform-limited pulses.

The pump and seed beams were focused into the center of a 1 m long gas cell using lenses with identical focal lengths. Collinear spatial alignment was achieved via a dichroic mirror (DM; HR @ 1030 nm / HT @ 1700-2400 nm), while the precise temporal overlap of the pulses was controlled using a delay line (DL). To determine the optimal focusing conditions, lenses with focal lengths of 500, 750, 1000, and 1500 mm were tested. For the seed beam, CaF_2 lenses were utilized. The 500 mm focal length lens was found to be unsuitable because the high intensity induced air plasma generation before the SRS threshold could be reached. Conversely, with the 1500 mm focal length lens, the maximum pump pulse energy was limited to 1 mJ due to the small beam size at the cell windows (increasing the risk of optical damage). No significant differences in the SRS threshold or conversion efficiency were observed between the 750 mm and 1000 mm focal length lenses. All results presented in this work were obtained using the 750 mm focal length lens to ensure a larger beam diameter at the cell windows. Following SRS excitation in the compressed hydrogen cell, conversion efficiency measurements and output spectral analysis were performed to optimize the gas pressure and pump pulse energy for maximum first-order Stokes generation. In this study, the SRS threshold is defined as the input pulse energy required to reach a 1% conversion efficiency.

4. Measurement methodology

4.1. Pulse width measurement

In order to fully characterize ultrashort pulses, measurements in the time and frequency domains are required. Thus, we used frequency-resolved optical gating (FROG) method [60]. The principle of FROG measurement is based on the autocorrelation of the pulse being measured; as the pulses overlap in space and time, changes are recorded depending on the type of interaction. In this work, the Stokes pulses were measured using a laboratory-built second-harmonic generation frequency-resolved optical gating (SHG-FROG) setup.

The pulses are overlapped in a 250 μm thick lithium iodate ($LiIO_3$) crystal, and the second-harmonic spectrum is recorded using an Avantes AvaSpec-ULS3648 spectrometer (covering the 432-980 nm spectral range) with a resolution of 1.1-1.3 nm. Once the complete spectrogram (FROG trace) is measured, the temporal and spectral envelopes and phases are reconstructed using a difference map algorithm.

4.2. Pulse energy measurement

Pulse energies were measured using an Ophir StarBright power meter equipped with an Ophir PE9-ES-C pyroelectric sensor, which features a spectral range of 0.15-3 μm and a measurement range of 0.1-200 μJ. For higher energy pulses, a Coherent LabMax-TOP meter with a J-10MT-10kHz EnergyMax sensor was utilized (spectral range: 0.19-12 μm; measurement range: 0.01-100 mJ). The spectral sensitivity of these sensors is well-suited for measuring both the pump and Stokes pulse energies. The experimental layout for energy measurements is shown in Fig. 6. For Stokes pulse energy measurements (Fig. 6a), a dichroic mirror (DM) was employed to reflect the pump radiation, combined with a long-pass spectral filter (F) to transmit wavelengths above 1050 nm (FELH 1050, Thorlabs). To isolate the anti-Stokes pulse energy (Fig. 6b), a short-pass spectral filter (F) with a cut-off below 1000 nm was used (FESH 1000, Thorlabs).

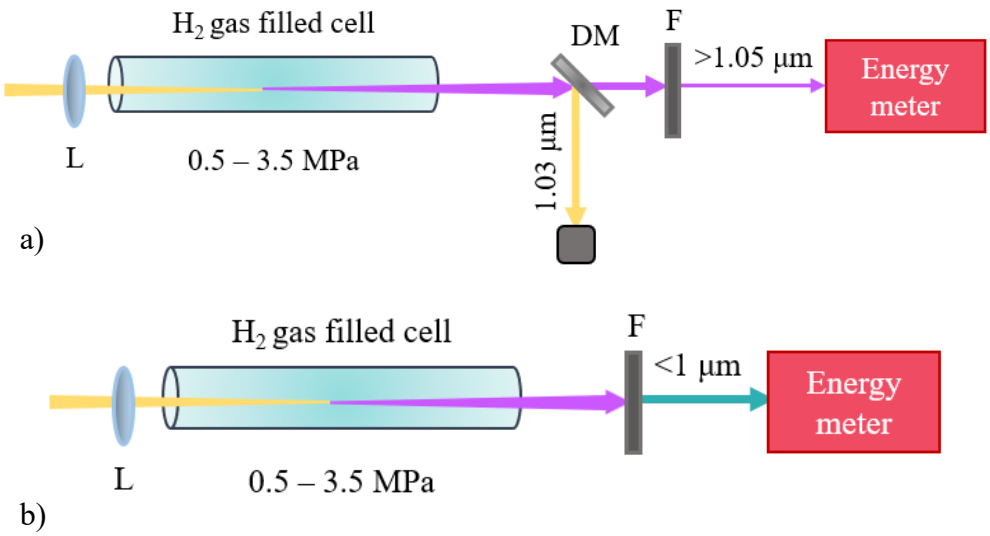

Fig. 6. Experimental setup for a) Stokes and b) anti-Stokes pulse energy measurement. L – focusing lens, DM – dichroic mirror, F – interference filter.

4.3. Pulse spectral envelope measurement

The spectral envelope of the Stokes pulses was measured using an Avesta ASP-IR-3.5 spectrometer (covering the 1100-3500 nm spectral range). At the output of the gas cell, the pump (1030 nm) and Stokes (1800 nm) radiation were separated by a dichroic mirror (Fig. 7., DM). To prevent nonlinear effects in the optical fiber at higher pulse energies, a neutral density filter (NDF) was placed before the fiber input. Following the NDF, a long-pass spectral filter (FELH 1050, Thorlabs) was installed to transmit only wavelengths above 1050 nm.

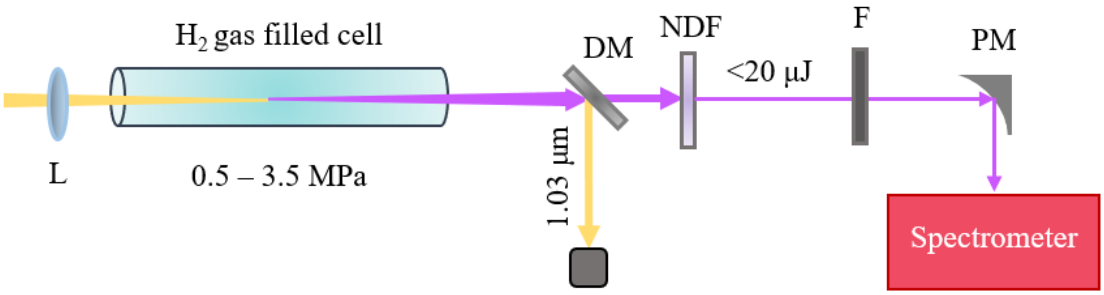

Fig. 7. Experimental setup for spectrum measurements. L – focusing lens, DM – dichroic mirror, NDF – neutral density filter, F – interference filter, PM – 45° silver-coated parabolic mirror.

Anti-Stokes spectra were recorded using an Avantes AvaSpec-ULS3648 spectrometer (432-980 nm range) with a resolution of 1.1-1.3 nm. To isolate these signals, a short-pass filter transmitting radiation below 1000 nm (FESH 1000, Thorlabs) was positioned before the fiber input.

The spectral envelope of the pump pulses was measured using an Ando AQ-6315A spectrum analyzer (covering the 350-1750 nm spectral range) with a resolution of 0.05 nm.

4.4. Beam profile measurement

The spatial profiles of the amplified Stokes radiation were recorded using a DataRay WinCamD-LCM CMOS camera. Since the sensor's spectral sensitivity (355-1150 nm) does not cover the Stokes wavelength, the beam was focused onto the sensor to visualize the profile via two-photon absorption (TPA).

The anti-Stokes beam profiles were captured using a digital camera.

For the spatial alignment of the seed and pump beams, a Xeva 1.7 320 InGaAs camera was utilized (spectral sensitivity: 900-1700 nm).

5. Results and discussion

5.1. Stimulated Raman amplification of a seed signal

Initially, the 1030 nm pump beam was focused into the pressurized hydrogen cell, and the SRS generation threshold was determined by increasing the pulse energy from 0.1 mJ. The gas pressure was set to the maximum value of 3.5 MPa. Vibrational Stokes radiation at 1.8 μm was observed at a pump pulse energy of approximately 0.9 mJ. As the energy was further increased, changes in the SRS spectrum were recorded (Fig. 8a). While initially increasing the pump pulse energy improved the conversion efficiency, at 1.7 mJ, the vibrational Stokes pulse began to trigger rotational Stokes radiation at 2 μm, corresponding to the 587 cm^{-1} rotational Raman shift in H_2. Subsequently, anti-Stokes radiation at 1.6 μm was also observed. The conversion efficiency reached only 1.5% (Fig. 9a, red curve), with a maximum vibrational Stokes pulse energy of 25 μJ. table shows a sharp decline at higher energies, where competing nonlinear effects becomes dominant: the pump generates a white-light supercontinuum, as shown in the beam profile photograph inset in the graph. Furthermore, multiple orders of anti-Stokes pulses were generated (Fig. 8b), which in turn triggered additional rotational Stokes components.

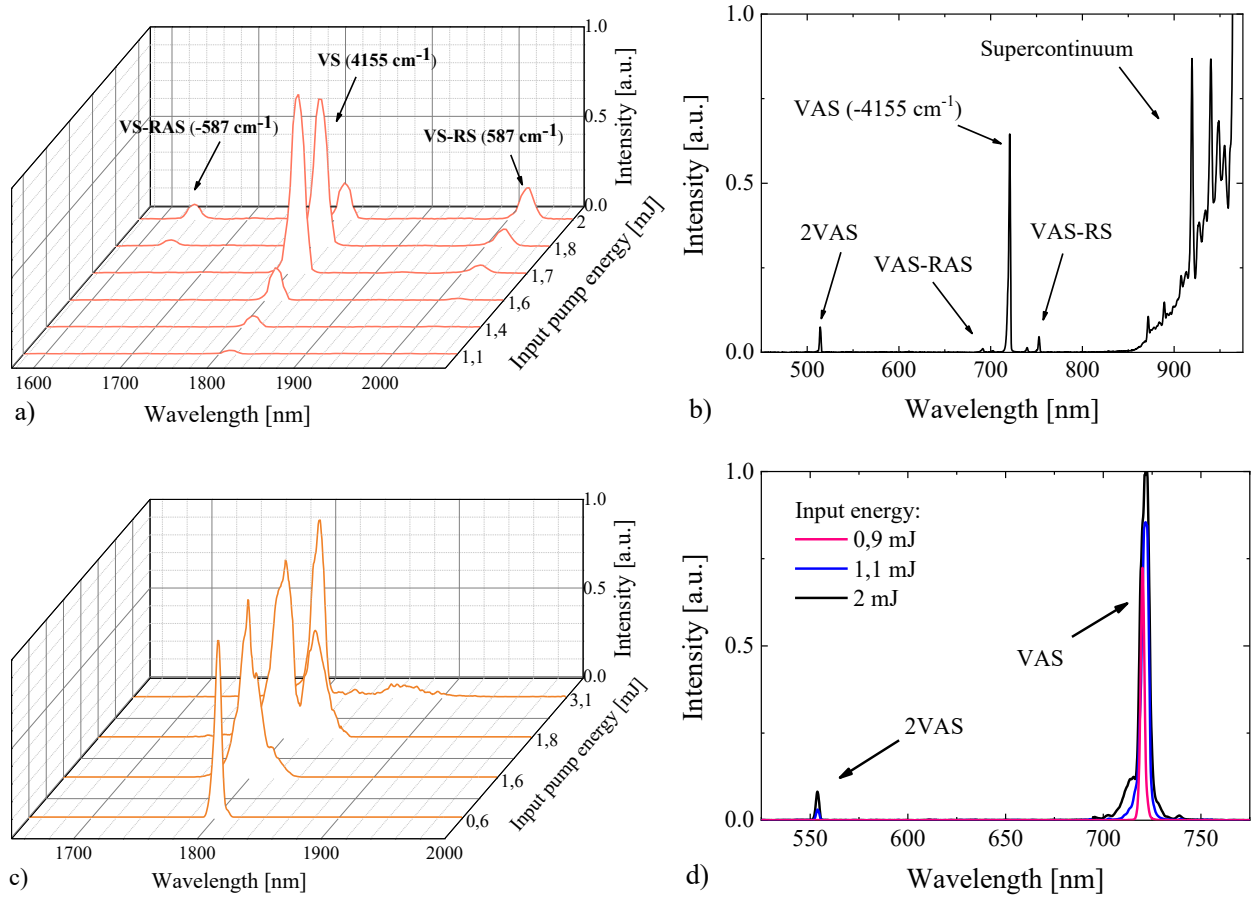

Fig. 8. SRS spectral profiles using different input pump pulse energy in the case of a) non-seeded SRS and c) seeded SRA. Spectral profiles in the visible spectral range (anti-Stokes) in the case of b) non-seeded SRS using pump pulse energy of 1.8 mJ and d) seeded SRA using different pump energies. VS – vibrational Stokes, VS-RAS – rotational anti-Stokes from vibrational Stokes, VS-RS – rotational Stokes from vibrational Stokes, VAS – vibrational anti-Stokes.

As anticipated, high conversion efficiency was not achievable in the transient Raman scattering regime; beyond a pump pulse energy of 1.8 mJ, the efficiency began to decline (Fig. 8a) due to competing nonlinear effects. Consequently, the experimental setup was transitioned to a seeded SRS (SRA) configuration (Fig. 5).

A supercontinuum generated in a YAG crystal served as the seed source, which was spectrally filtered using an AOPDF to match the central wavelength of the vibrational Stokes radiation. The spectral width was limited to 100 nm at FWHM in order to prevent unwanted seeding of rotational Stokes. The pump and seed pulses were synchronized in time, aligned spatially, and focused into the center of the H_2 gas cell at a pressure of 3.5 MPa. The Stokes pulse energy was measured as a function of pump pulse energy, and the resulting conversion efficiency curve is presented in Fig. 9a. Using a pump pulse energy of 1.2 mJ, a maximum conversion efficiency of 30.2% was achieved (quantum efficiency of 52.8%), yielding a Stokes pulse energy of 370 µJ. The Stokes beam profile remained undistorted, exhibiting a Gaussian distribution.

The seed not only enhanced the conversion efficiency but also reduced the SRS generation threshold by a factor of six: a 1% conversion efficiency was reached at just 0.2 mJ, whereas 1.2 mJ was required in the unseeded regime. Furthermore, the threshold for supercontinuum generation increased by approximately 1.5 times, as vibrational SRS became the dominant nonlinear process. In the unseeded regime, the vibrational and rotational Raman modes compete for the available pump pulse energy (Fig. 8a, b). However, the introduction of the seed provides a significant initial photon density for the vibrational transition at 1.8 μm. This leads to rapid pump depletion into the vibrational channel, preventing the competing rotational transition (587 cm^{-1} shift) from reaching its threshold. Consequently, the SRA configuration yields a much cleaner spectral output by effectively suppressing parasitic rotational components (Fig. 8c, d).

Observation of the visible beam profiles (Fig. 9a, insets) shows a single red ring before the saturation point, corresponding to first-order anti-Stokes radiation at 720 nm central wavelength. Upon reaching saturation, a green ring appears (second-order anti-Stokes at 554 nm central wavelength), followed by a blue ring (third-order anti-Stokes at 450 nm central wavelength), eventually leading to the onset of white-light supercontinuum generation. The presence of these higher-order anti-Stokes components supports the assumption that higher-order Stokes pulses are also being generated. The central wavelength of the second-order Stokes radiation is estimated to be approximately 7.15 μm; however, due to the lack of suitable detection equipment for this spectrum range, the focus of the subsequent analysis remains on the first-order Stokes pulses.

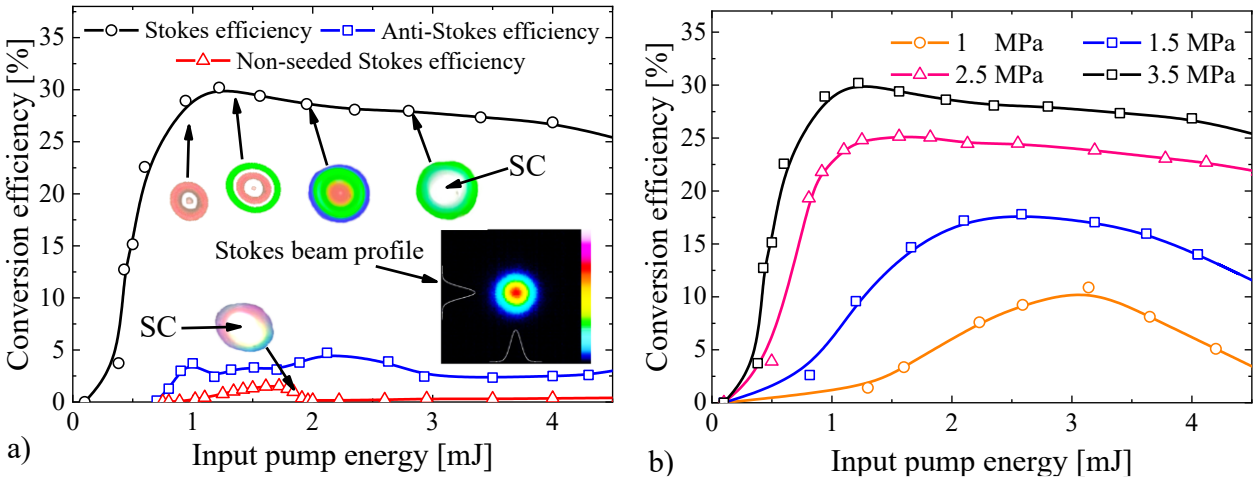

Fig. 9. a) Dependence of SRA Stokes (black curve, circles), anti-Stokes (blue curve, squares) and SRS Stokes pulse conversion efficiency on input pump pulse energy. SC – supercontinuum. Insets – photographs of the beam in the visible spectral range (anti-Stokes) and Stokes beam profile measured via TPA. b) Dependence of SRA conversion efficiency on the input pump pulse energy using different hydrogen pressure.

Conversion efficiency curves were also measured with different hydrogen pressures (Fig. 9b). Decreasing the H_2 pressure in the cell leads to an increase in the SRS threshold and a reduction in the maximum achievable conversion efficiency. When the pressure was reduced from 3.5 MPa to

0.5 MPa, the threshold increased nearly eightfold, while the maximum conversion efficiency decreased by a factor of 3.6. Notably, at the minimum pressure of 0.5 MPa, supercontinuum generation began before the Stokes pulse could reach conversion saturation. Spectral envelopes were also compared for pressures ranging from 3.5 MPa to 1 MPa at similar points along the efficiency curves – specifically before, near, and well beyond the saturation point. The spectrum remained similar across all pressures.

The Stokes pulse spectrogram was measured, and a full pulse characterization was obtained via FROG retrieval. The pulse envelope (solid black curve), temporal phase (dashed curve), and the measured and retrieved spectrograms are presented in Fig. 10a. The measured (black curve) and retrieved (red curve) spectral envelopes, along with the spectral phase (dashed curve), are shown in Fig. 10b. The FROG retrieval error was 0.36% RMS with a grid size of 512×512. During this measurement, a pump pulse energy of 0.9 mJ was selected to ensure the conversion efficiency approached saturation (Fig. 9a) without triggering second-order Stokes generation. The conversion efficiency at this point reached ~28% (corresponding to a quantum efficiency of 49%), with a Stokes pulse energy of approximately 250 μJ. Pulse shape is consistent with typical Stokes pulse characteristics [20], exhibiting an asymmetric profile with a steep front. The Stokes pulse is 2.3 times shorter than the pump pulse, with a duration of 575 fs. The measured Stokes pulse spectrum corresponds to a transform-limited duration of 573 fs (Fig. 10b, inset), indicating that the retrieved 575 fs pulse is nearly transform-limited.

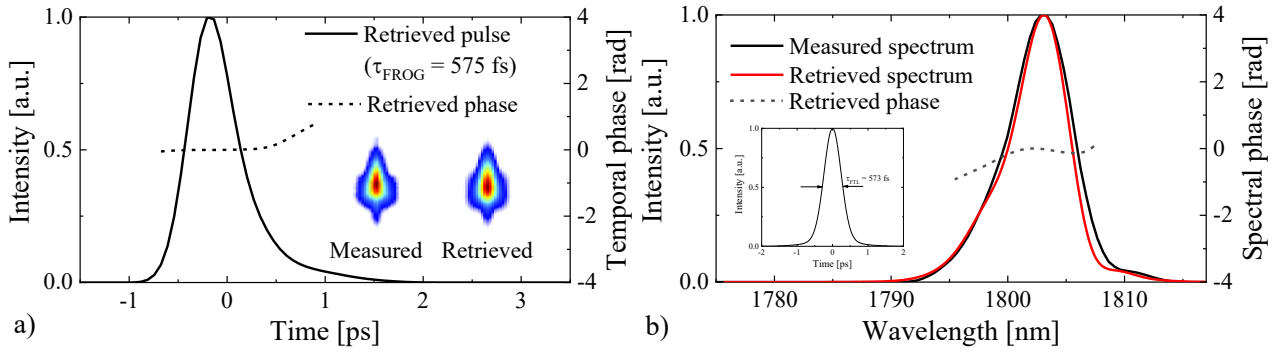

Fig. 10. a) Temporal profile (solid) and temporal phase (dashed); b) measured (black), retrieved (red) spectral profiles and spectral phase (dashed) of the Stokes pulse retrieved from SHG-FROG measurements for temporally overlapped WLC seed. Insets: a) measured and retrieved FROG traces with <1% error using a 512×512 grid; b) FTL temporal shape calculated from the measured spectra of the Stokes pulse.

The output pump spectrum was measured to get an understanding of why the Stokes pulse is shorter than the initial pump pulse duration. Input pump spectrum and output pump spectra with different input energies are shown in Fig. 11 for SRS and SRA. In the seeded regime (Fig. 11b), the pump spectrum exhibits extreme asymmetric broadening toward longer wavelengths, far exceeding the broadening observed in the unseeded case (Fig. 11a). This could be attributed to the rapid growth

of the Stokes pulse as well as the temporal steepening of the pump's trailing edge; both characteristics are consistent with operation in a transient Raman scattering regime. At higher pump pulse energies, the pump spectrum was significantly broadened toward longer wavelengths and eventually approaching complete depletion of the spectral intensity at the initial central wavelength of 1030 nm.

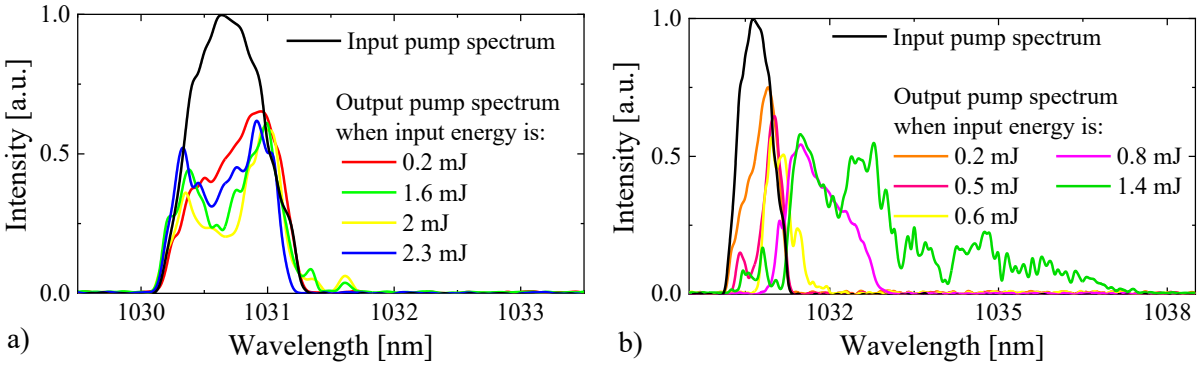

Fig. 11. Input (black) and output pump spectral profiles in case of a) non-seeded SRS and b) seeded SRS using different input pump pulse energy.

In order to see how the Stokes pulse spectrum broadened relatively to the pump pulse we can plot their spectra in wavenumbers. Firstly, the wavelength was converted to absolute wavenumbers [cm^{-1}]:

$$\tilde{\nu}_{absolute} = \frac{1}{\lambda}. \tag{5}$$

The Raman shift (4155 cm^{-1}) was applied to the Stokes pulse data, and the pump pulse central wavelength was set as 0. The received spectral mapping is shown in Figure 12. The Stokes spectrum is three times broader than the input pump spectrum which is a clear visual indicator of SPM and transient SRS dynamics.

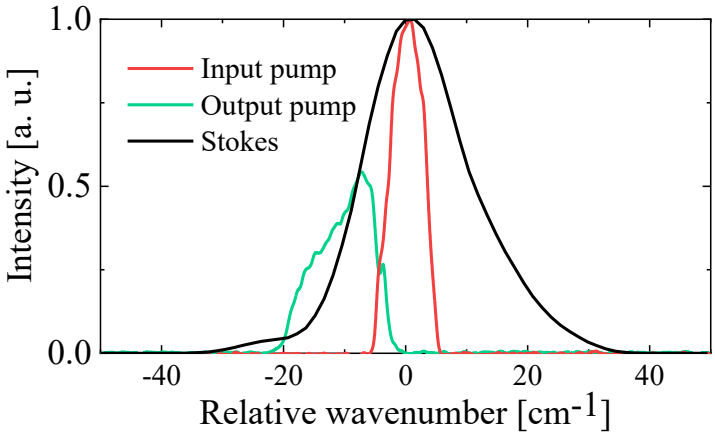

Fig. 12. Normalized spectra of the 1.03 µm input and output pump and the 1.8 µm vibrational Stokes signal mapped to a relative wavenumber axis. The Stokes spectrum is shifted by the Raman vibrational mode of hydrogen (4155 cm^{-1}) to facilitate a direct comparison of spectral broadening and pump depletion.

As the results demonstrate, the SRA configuration in a high-pressure hydrogen gas cell is highly efficient, achieving a quantum conversion efficiency of 53%. This setup generated near-transform-limited 575 fs first-order Stokes pulses that are centered at 1.8 μm wavelength. To maintain a smooth temporal profile, we need to operate the system at pump energies below the conversion saturation threshold, beyond which the first-order Stokes pulse is depleted due to energy transfer into higher-order Stokes components. The spectrum and duration of Stokes pulses remained consistent over the entire tested range of hydrogen pressure (0.5-3.5 MPa), even though the conversion efficiency decreased at lower pressures.

As we see from SRS spectral profiles in Fig. 8c, with increasing pump pulse energy it is possible to get an even broader Stokes spectra. However, when the conversion efficiency saturation is reached, the first-order Stokes pulse is depleted due to second-order Stokes generation. Thus, if we want to use more energy of the pump pulse and get a shorter, non-depleted broadband Stokes pulse, we should decrease the SRS efficiency below the second-order Stokes pulse generation threshold. This can be done by decreasing the pressure of hydrogen; however, as seen from the experiments, at saturation point, the Stokes spectrum bandwidth with different pressures is almost identical. That could be explained by the fact that decreasing pressure decreases the nonlinear refractive index of the medium and thus the threshold of nonlinear effects is also changed. Another possible way to decrease the SRS conversion efficiency while maintaining the same nonlinear refractive index is changing the temporal overlap between pump and seed pulses.

5.2. Controlling the balance between nonlinear effects

To achieve further shortening of the Stokes pulse, we sought a balance between competing nonlinear effects by tuning the pump-seed temporal delay. Whereas the nonlinear response of the medium is related to vibrational dephasing time ($T_2 \approx 250\ ps$), we can expect that SRA would still be excited even without the temporal overlap between seed and pump pulses. It is expected that the conversion efficiency would drop when the pulses are not temporally overlapped and, in this case, we could use more energy of the pump pulse without reaching the threshold of second-order Stokes generation. The spectrum should broaden a lot more due to SPM and the first-order Stokes pulse would not be depleted.

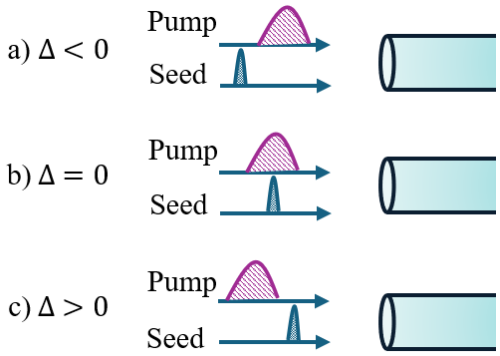

Fig. 13. Schematic diagram of the relative temporal delay between pump and seed pulses. Positive delay *Δ* corresponds to the case when the seed pulse comes before the pump pulse.

The pump pulse was temporally delayed in respect of the supercontinuum seed (Fig. 13). The dependence of SRA conversion efficiency and Stokes pulse duration on the pump-seed temporal delay is presented in Figure 14. The maximum SRA conversion efficiency was achieved when the seed and pump pulses temporally overlapped. In case when the pump pulse comes before the seed pulse, the conversion efficiency drops sharply, and only non-seeded SRS with a conversion efficiency of ~1 % is observed. When the pump pulse comes after the seed, conversion efficiency drops sharply from 27.6% to 17% over 5 ps delay and then decays to 15% in 80 ps.

The Stokes pulse duration was measured simultaneously (Fig. 14b). When the input pump pulse energy is 1.7 mJ, and the pulses are temporally overlapped, we observe significant spectral broadening of the output pump spectrum; however, the Stokes pulse was depleted due to the second-order Stokes generation. As the pump-seed temporal delay was increased, the Raman gain dropped thus stopping the generation of second-order Stokes component but allowing the pump spectrum sufficiently broaden via SPM and thus we obtained short, non-depleted Stokes pulse. Temporal delay also allows the pump to arrive when the vibrational coherence in the medium is fully established but has not yet decayed.

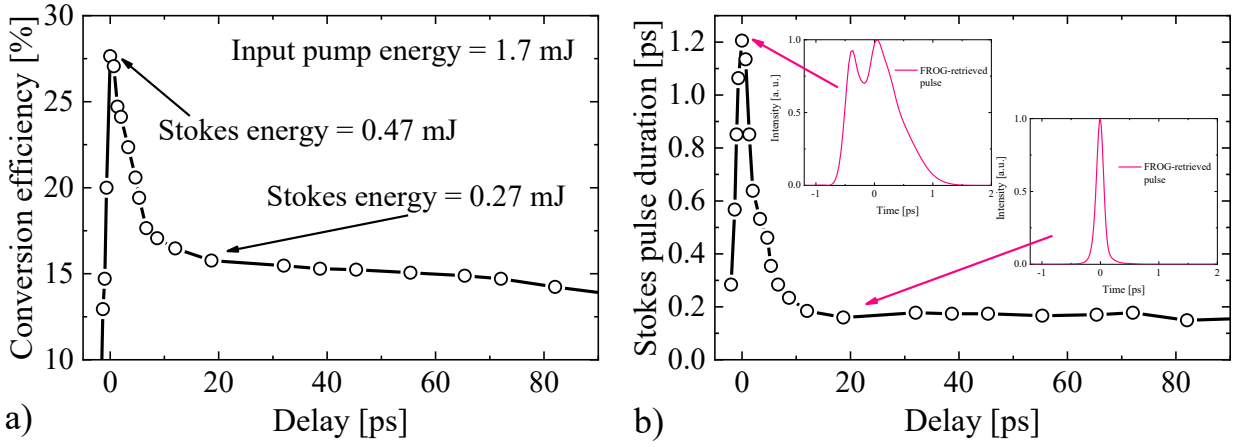

Fig. 14. Dependence of a) conversion efficiency and b) Stokes duration on the pump-seed delay. Insets in b) are FROG-retrieved Stokes pulses when the pump and seed are temporally overlapped and when the pump is delayed by 20ps.

The spectrogram of the Stokes pulse in case of temporally delayed pump was measured, and a full pulse characterization was obtained via FROG retrieval. The pulse envelope (solid black curve), temporal phase (dashed curve), and the measured and retrieved spectrograms are presented in Fig. 15a. The measured (black curve) and retrieved (red curve) spectral envelopes, along with the spectral phase (dashed curve), are shown in Fig. 15b. The FROG retrieval error was 0.3% RMS with a grid size of 512×512. The efficiency reached ~15.9% (corresponding to a quantum efficiency of 28%), with a Stokes pulse energy of approximately 270 μJ. The Stokes pulse in this case is almost 4 times shorter than in the case of temporally overlapped seed-pump, with a duration of 146 fs. The measured Stokes pulse spectrum corresponds to a transform-limited duration of 145 fs (Fig. 15b, inset), indicating that the retrieved pulse is transform-limited. The total group delay dispersion (GDD) in this spectral region is estimated at ~74 fs^2, arising from the 1 m hydrogen path and two 5 mm CaF_2 windows of the cell. Given the negligible group velocity dispersion (GVD) of hydrogen (0.16 fs^2/mm), the spectrally broadened pulses remain near the transform limit, eliminating the need for pulse-compression stages.

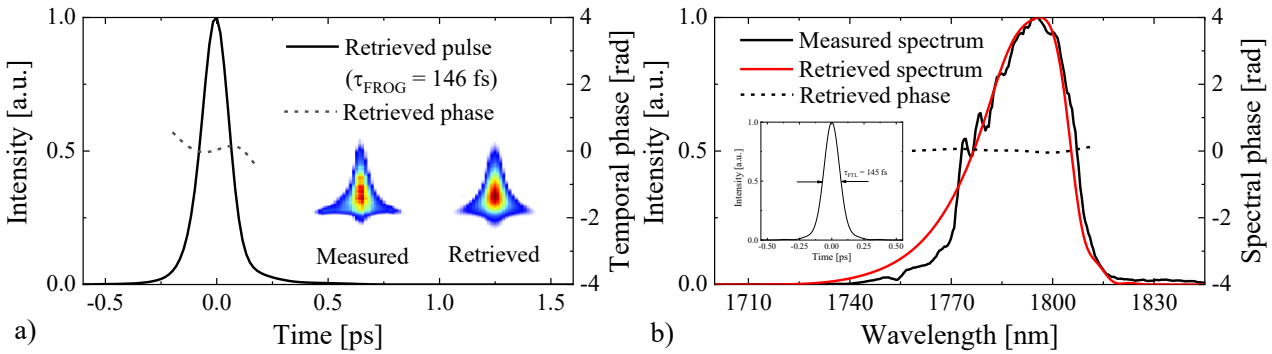

Fig. 15. a) Temporal profile (solid) and temporal phase (dashed); b) measured (black), retrieved (red) spectral profiles and spectral phase (dashed) of the Stokes pulse retrieved from SHG-FROG measurements for temporally delayed WLC seed. Insets: a) measured and retrieved FROG traces with <1% error using a 512×512 grid; b) FTL temporal shape calculated from the measured spectra of the Stokes pulse.

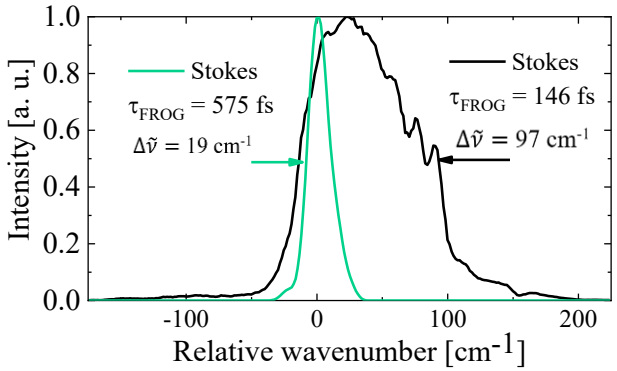

Fig. 16. Normalized spectra of the 1.8 μm vibrational Stokes signal mapped to a relative wavenumber axis. Green – overlapped pump and seed pulses, black – temporally delayed pump pulse. The Stokes spectrum is shifted by the Raman vibrational mode of hydrogen (4155 cm^{-1}) to facilitate a direct comparison of spectral broadening and pump depletion.

From the results obtained during the research, we can calculate the time-bandwidth product ($K = \Delta\tau \cdot c \cdot \Delta\tilde{\nu}$), which shows the relationship between the measured pulse duration and the spectral width of the Stokes signal. This value is critical for determining the pulse shape and identifying the presence of residual chirp, for an ideal Gaussian pulse $K = 0.441$. At a pump pulse energy of 0.9 mJ with temporally overlapped pulses, the system generated a 575 fs Stokes pulse with a 19 cm^{-1} bandwidth, resulting in $K \approx 0.327$. This value is below the Gaussian limit and sits closer to $sech^2$ profile ($K = 0.315$), which indicates a highly asymmetric, steep-fronted profile confirmed by FROG measurements. In the context of SRS, this is a signature of the transient regime, where the Stokes signal must wait for the pump to build up vibrational coherence in the hydrogen, leading to preferential amplification of the trailing edge and a characteristic sharpening of the pulse front.

Increasing the pump pulse energy to 1.7 mJ and delaying it relative to the seed allowed the spectral bandwidth to broaden five-fold to 97 cm^{-1}. The resulting K value of 0.425 is very close to the transform-limited Gaussian. This suggests that the temporal delay allows the Stokes signal to interact more effectively with the pre-excited material vibrations. This mitigates the non-instantaneous response of the transient process, maximizing spectral broadening while maintaining nearly transform-limited profile.

The future research will focus on increasing the repetition rates of the system to levels suitable for practical use in laser processing. In addition to addressing thermal accumulation and density perturbations in the hydrogen, we plan to implement an additional nonlinear compression stage using an argon filled gas cell that will broaden the spectrum of the Stokes pulse via self-phase modulation and thus enable us to obtain high energy pulses in the SWIR range with durations approaching the few-cycle regime.

6. Conclusions

In this work, we demonstrate that transient stimulated vibrational Raman scattering in compressed hydrogen provides an alternative route to generate SWIR femtosecond pulses. Driven by ~1.3 ps pump pulses at 1030 nm, the white light supercontinuum seeded transient SRS achieves conversion efficiencies exceeding 30%. After optimization, near transform limited 575 fs Stokes pulses at 1.8 μm with energies up to 0.25 mJ were obtained. By tuning the temporal delay between the pump and seed pulses, pulse shortening to 146 fs was achieved without the need of additional pulse-compression stages.

Summarizing the investigation results, the following conclusions were formulated:

1. In the transient SRS regime, rotational Stokes and anti-Stokes generation and supercontinuum generation suppresses efficient vibrational SRS, maximum conversion efficiency reached only 1.5%.
2. White light continuum seed (spectrally filtered with AOPDF) allows 6-fold reduction of SRS threshold and the conversion efficiency is increased 20 times reaching 30%. One can obtain a smooth Stokes pulse envelope before depletion to higher-order Stokes, i.e., before conversion efficiency saturation. Stokes pulse with a central wavelength of 1.8 μm, an energy of 250 μJ, and duration of 575 fs was obtained, the Stokes beam has no spatial distortions.
3. The higher hydrogen gas pressure in the cell allows to reduce the threshold of SRS generation and achieve higher efficiency, however it does not affect the duration of the Stokes pulses.
4. The temporal delay between the pump and seed pulses allowed to balance SPM and SRS processes and obtain nearly transform-limited 146 fs Stokes pulse with 15.9% conversion efficiency corresponding to an energy of 270 μJ.
5. While the pump peak power was 1.23 GW, the optimized 146 fs Stokes pulse reached a peak power of 1.91 GW. This enhancement occurs because the temporal shortening factor (~9 times) outweighs the energy conversion losses, demonstrating the capability of the hydrogen-filled cell to generate SWIR radiation exceeding the peak intensity of the driving laser.

Publications

Scientific articles:

1. A.M. Rodin, **A. Černeckytė**, P. Mackonis and A. Petrulėnas, Optimizing self-seeded perfluorooctane SBS-compressor configurations to achieve 90 ps high-energy pulses, Photonics, **10**(9), 1060, (2023).
2. A. Petrulenas, P. Mackonis, A. M. Rodin and **A. Černeckytė**, Cost-effective femtosecond laser source at 1800 – 3400 nm wavelengths based on multistage nonlinear conversion, Proc. SPIE, **12092**, Laser Technology for Defense and Security XVII, 1209204, (2022).
3. A. Petrulėnas, P. Mackonis, **A. Černeckytė**, A. M. Rodin, Amplification of supercontinuum seed pulses at ~1078–1355 nm by cascade rotational SRS in compressed hydrogen, Applied Sciences, **13**, 13087 (2023).
4. A. Petrulėnas, **A. Černeckytė**, P. Mackonis, A. M. Rodin, Combining OPCPA with transient rotational SRS in hydrogen for spectral extension to 3 μm, Opt. Commun., **592**, 132209, (2025).

Conference presentations:

1. **A. Černeckytė**, P. Mackonis, A.M. Rodin, Comparison of self-seeded Perfluorooctane SBS-compressor configurations for obtaining high-energy 90 ps pulses, 2023 Conference on Lasers and Electro-Optics Europe & European Quantum Electronics Conference (CLEO/Europe-EQEC), Munich, Germany, 26-30 June 2023. https://doi.org/10.1109/CLEO/Europe-EQEC57999.2023.10232741 (Poster)
2. **A. Černeckytė**, A. Petrulėnas, P. Mackonis, A.M. Rodin, Excitation of cascaded stimulated rotational Raman scattering by single-picosecond laser pulses, 45-oji Lietuvos nacionalinė fizikos konferencija, 2023 m. lapkričio 25-27d. Vilnius; ISBN 978-609-07-0981-8, pp. 228 https://doi.org/10.15388/LNPC.2023 (Poster)
3. **A. Černeckytė**, P. Mackonis and A.M. Rodin, High energy 90 ps pulses from Perfluorooctane SBS-compressor, 66th International Conference for Students of Physics and Natural Sciences "Open Readings'2023", 18–21 April 2023, Vilnius, pp. 243 https://openreadings.eu/wp-content/abstracts/abstract-2023.pdf (Award for the best poster presentation)
4. **A. Černeckytė**, P. Mackonis, A.M. Rodin, Priešpriešiai kaupinimui sklindančių lazerio impulsų spūda taikant priverstinę Brillouino sklaidą, 11-oji Jaunųjų Mokslininkų Konferencija „Fizinių ir technologijos mokslų tarpdalykiniai tyrimai", 2023 m. kovo 23d. Vilnius pp. 4 https://www.lma.lt/uploads/Pranesimai%20naujienoms/11_JM%20konferencijos_pranesimu_santraukos_1.pdf (Poster)
5. **A. Černeckytė**, A. Petrulėnas, P. Mackonis, A.M. Rodin, High-Efficiency mid-IR OPCPA with 2.5 mj 25 fs Output Pulses, 67th International Conference for Students of Physics and Natural

Sciences "Open Readings'2024", 23–26 April 2024, Vilnius, pp. 60 https://openreadings.eu/wp-content/uploads/2024/05/2024_abstract_book.pdf (Oral)

6. **A. Černeckytė**, A. Petrulenas, P. Mackonis and A.M. Rodin, Excitation of a stimulated rotational Raman scattering comb in a hydrogen cell, 7th International Conference on Optics, Photonics and Lasers (OPAL' 2024), 17–19 May 2024, Palma de Mallorca, Mallorca (Balearic Islands), Spain, ISBN: 978-84-09-61372-4. http://dx.doi.org/10.13140/RG.2.2.20925.27360 (Award for the best oral presentation)
7. **A. Černeckytė**, A. Petrulėnas, P. Mackonis and A.M. Rodin, Cost-effective few-cycle mJ-level laser at 1800–2650 nm based on OPCPA and rotational SRS in hydrogen, Extreme Light Infrastructure Summer School 2024 (ELISS 2024) 2 – 6 September 2024, Szeged, Hungary, pp. 36 https://indico.eli-laser.eu/event/48/attachments/167/1005/ELISS_2024_abstract_book.pdf (Poster)
8. **A. Černeckytė**, A. Petrulėnas, P. Mackonis and A. M. Rodin, Generation of Intense Femtosecond Pulses Beyond 3000 nm Using OPCPA Combined with Transient Rotational SRS in Hydrogen, 2025 Conference on Lasers and Electro-Optics Europe & European Quantum Electronics Conference (CLEO/Europe-EQEC), Munich, Germany, 2025, DOI: 10.1109/CLEO/Europe-EQEC65582.2025.11111349 (Oral)
9. **A. Černeckytė**, A. Petrulenas, P. Mackonis and A.M. Rodin, Excitation of a stimulated rotational Raman scattering comb in a hydrogen cell, 8th International Conference on Optics, Photonics and Lasers (OPAL' 2025), 14-16 May 2025, Rhodes, Greece, pp. 69-71 DOI: 10.13140/RG.2.2.10223.96166 (Oral)
10. **A. Grigaravičienė,** P. Mackonis, and A. M. Rodin, Two-stage hybrid Yb:YAG / Yb:LuAG ultra-high gain chirped pulse amplifier, 9th International Conference on Optics, Photonics and Lasers (OPAL' 2026), 20-22 May 2026, Ibiza (Balearic Islands), Spain.

Co-author of conference presentations:

1. A. Petrulenas, P. Mackonis, **A. Černeckytė** and A.M. Rodin, High-energy few-optical-cycle multispectral NIR-SWIR-MIR laser based on OPCPA and stimulated Raman scattering, Proceedings of the 6th International Conference on Optics, Photonics and Lasers (OPAL' 2023), 17-19 May 2023, Funchal (Madeira Islands), Portugal, pp. 98-100, ISBN: 978-84-09-48335-8.
2. **A. Černeckytė**, P. Mackonis, A.M. Rodin, Laser with SBS-compression and phase-conjugation in Perfluorooctane for interference patterning, Proceedings of the 6th International Conference on Optics, Photonics and Lasers (OPAL' 2023), 17-19 May 2023, Funchal (Madeira Islands), Portugal, pp. 119-121, ISBN: 978-84-09-48335-8.

3. A. Petrulenas, P. Mackonis, **A. Černeckytė** and A.M. Rodin, Didelės energijos kelių optinių ciklų NIR-SWIR-MIR diapazono lazerinė sistema, 13-oji FTMC Doktorantų ir Jaunųjų Mokslininkų konferencija, Vilnius, 18-19 October 2023.
4. A. Petrulėnas, **A. Černeckytė**, P. Mackonis, and A.M. Rodin, High-efficiency BiBO-based OPCPA with ~2.2 mJ output pulses at ~2.2 μm compressed to 25 fs, in High-Brightness Sources and Light-Driven Interactions Congress, Technical Digest Series (Optica Publishing Group, 2024), paper HTu5B.1. https://doi.org/10.1364/HILAS.2024.HTu5B.1
5. P. Mackonis, A. Petrulėnas, **A. Černeckytė**, and A.M. Rodin, Amplification of supercontinuum Seed Pulses at 1.1–1.4 μm by cascade rotational SRS in compressed hydrogen, in High-Brightness Sources and Light-Driven Interactions Congress, Technical Digest Series (Optica Publishing Group, 2024), paper JTu4A.20. https://doi.org/10.1364/EUVXRAY.2024.JTu4A.20
6. A. Petrulenas, P. Mackonis, **A. Černeckytė** and A.M. Rodin, Recent advances in the development of few-cycle Mid-IR Laser based on OPCPA and SRRS, Proceedings of the 7th International Conference on Optics, Photonics and Lasers (OPAL' 2024), 17–19 May 2023, Palma de Mallorca, Mallorca (Balearic Islands), Spain., pp. 65–67, ISBN: 978-84-09-61372-4. http://dx.doi.org/10.13140/RG.2.2.20925.27360
7. P. Mackonis, **A. Černeckytė**, A. Petrulėnas, A.M. Rodin and D. Klumbys, High-energy dual-channel four-pass phase-conjugated Nd:YAG amplifier with SBS pulse compression for interference patterning, Proceedings of the 7th International Conference on Optics, Photonics and Lasers (OPAL' 2024), 17–19 May 2023, Palma de Mallorca, Mallorca (Balearic Islands), Spain., pp. 152–153, ISBN: 978-84-09-61372-4. http://dx.doi.org/10.13140/RG.2.2.20925.27360
8. A.M. Rodin, A. Petrulėnas, P. Mackonis and **A. Černeckytė**, Economic aspects and technologies in the development of advanced cost-effective few-cycle sub-TW Class mid-IR Lasers, Proceedings of the 7th International Conference on Optics, Photonics and Lasers (OPAL' 2024), 17–19 May 2023, Palma de Mallorca, Mallorca (Balearic Islands), Spain., pp. 154–158, ISBN: 978-84-09-61372-4. http://dx.doi.org/10.13140/RG.2.2.20925.27360
9. D. Klumbys, P. Mackonis **A. Černeckytė,** A. Petrulėnas, A.M. Rodin, FOUR PASS DUAL CELL SBS-PCM AMPLIFIER, *67th International Conference for Students of Physics and Natural Sciences "Open Readings'2024", 23–26 April 2024, Vilnius*, pp. 137 https://openreadings.eu/wp-content/uploads/2024/05/2024_abstract_book.pdf
10. O. Myronyuk, A. M. Rodin and **A. Černeckytė**, Water Repellency of Laser-Textured Aluminum Surfaces Compared to its Polymer Imprints, 2025 Conference on Lasers and Electro-Optics Europe & European Quantum Electronics Conference (CLEO/Europe-EQEC), Munich, Germany, 2025, doi: 10.1109/CLEO/Europe-EQEC65582.2025.11111314.

11. P. Mackonis, **A. Grigaravičienė**, A. Rodin, and R. Pečiulytė, A self-compression approach for generating ~150 fs laser pulses in the SWIR range based on transient SRS, 9th International Conference on Optics, Photonics and Lasers (OPAL' 2026), 20-22 May 2026, Ibiza (Balearic Islands), Spain.
12. A. Rodin, A. Grigaravičienė, P. Mackonis, and R. Pečiulytė, 40 ps pulses at 1064 nm from SBS-compressor with trailing-edge reshaping by transient forward SRS, 9th International Conference on Optics, Photonics and Lasers (OPAL' 2026), 20-22 May 2026, Ibiza (Balearic Islands), Spain.

References

[1] M. Chambonneau, D. Grojo, O. Tokel, F. Ö. Ilday, S. Tzortzakis, and S. Nolte, In-Volume Laser Direct Writing of Silicon-Challenges and Opportunities, Laser Photon. Rev., **15**(11), (2021).

[2] T. Popmintchev, M. Chen, D. Popmintchev, P. Arpin, S. Brown, S. Ališauskas, G. Andriukaitis, T. Balčiunas, A. Pugzlys, A. Baltuška, A. Gaeta, A. Becker, M. Murmane, S. Schrauth, and H. Kapteyn, Bright Coherent Ultrahigh Harmonics in the keV X-ray Regime from Mid-Infrared Femtosecond Lasers, Science, **336**, 1287, (2012).

[3] C. Gollner, M Shalaby, C. Brodeur, I. Astrauskas, R. Jutas, E. Constable, L. Bergen, A. Baltuška, and A. Pugžlys, Highly efficient THz generation by optical rectification of mid-IR pulses in DAST, APL Photon., **6**(4), 046105 (2021).

[4] A. Petrulenas, P. Mackonis, and A. M. Rodin, High-efficiency bismuth borate-based optical parametric chirped pulse amplifier with approximately 2.1 mJ, 38 fs output pulses at approximately 2150 nm, High Power Laser Sci. Eng., **11**, e27, (2023).

[5] P. Gierschke, C. Grebing, M. Abdelaal, M. Lenski, J. Buldt, Z. Wang, T. Heuermann, M. Mueller, M. Gebhardt, J. Rothhardt, and J. Limpert, Nonlinear pulse compression to 51-W average power GW-class 35-fs pulses at 2-μm wavelength in a gas-filled multi-pass cell, Opt. Lett., **47**(14), 3511-3514, (2022).

[6] K. Murari, G. Cirmi, H. Cankaya, G. J. Stein, B. Debord, F. Gerome, F. Ritzkosky, F. Benabid, and F. X. Kartner, Sub-50 fs pulses at 2050 nm from a picosecond Ho:YLF laser using a two-stage Kagome-fiber-based compressor, Photonics Res., **10**(3), 637-645, (2022).

[7] E. R. Peck and S. Huang, Refractivity and dispersion of hydrogen in the visible and near infrared, J. Opt. Soc. Am., **67**(11), 1550, (1977).

[8] Y. H. Chen and F. Wise, Unified and vector theory of Raman scattering in gas-filled hollow-core fiber across temporal regimes, APL Photon., **9**(3), 030902, (2024).

[9] N. J. Everall, J. P. Partanen, J. R. M. Barr, and M. J. Shaw, Threshold measurements of stimulated Raman scattering in gases using picosecond KrF laser pulses, Opt. Commun., **64**(4), 393-397, (1987).

[10] V. Krylov, O. Ollikainen, U. P. Wild, A. Rebane, V. G. Bespalov, and D. I. Staselko, Femtosecond stimulated Raman scattering in pressurized gases in the ultraviolet and visible spectral ranges, J. Opt. Soc. Am. B, **15**(12), 2910-2916, (1998).

[11] H. M. Pask, The design and operation of solid-state Raman lasers, Prog. Quantum Electron., **27**, 3-56, (2003).

[12] S. Loranger, P. St. J. Russell, and D. Novoa, Sub-40 fs pulses at 1.8 μm and MHz repetition rates by chirp-assisted Raman scattering in hydrogen-filled hollow-core fiber, J. Opt. Soc. Am. B, **37**(12), 3550, (2020).

[13] Z. Wang, F. Yu, W. J. Wadsworth, and J. C. Knight, Efficient 1.9 μm emission in H2-filled hollow core fiber by pure stimulated vibrational Raman scattering, Laser Phys. Lett., **11**(10), (2014).

[14] A. Petrulėnas, P. Mackonis, A. Černeckytė, and A. M. Rodin, Amplification of Supercontinuum Seed Pulses at ~1078–1355 nm by Cascade Rotational SRS in Compressed Hydrogen, Appl. Sci., **13**(24), (2023).

[15] K. Li, C. Niu, C. Wu, Y. Yu, and Y. Ma, Development of a 2 μm Solid-State Laser for Lidar in the Past Decade, Sensors, **23**, 7024, (2023).

[16] R. A. Richter, N. Tolstik, S. Rigaud, P. D. Valle, A. Erbe, P. Ebbinghaus, I. Astrauskas, V. Kalashnikov, E. Sorokin, and I. T. Sorokina, Sub-surface modifications in silicon with ultra-short pulsed lasers above 2 μm, J. Opt. Soc. Am. B, **37**(9), 2543, (2020).

[17] R. Malik, B. Mills, J. H.V. Price, M. Petrovich, Z. Moktadir, Z. Li, and H. N. Rutt, Determination of the mid-IR femtosecond surface-damage threshold of germanium, Appl. Phys. A, **113**, 127–133, (2013).

[18] I. Pavlov, O. Tokel, S. Pavlova, V. Kadan, G. Makey, A. Turnali, O. Yavyz, and F. O. Ilday, Femtosecond laser written waveguides deep inside silicon, Opt. Lett., **42**(15), 3028, (2017).

[19] I. Astrauskas, B. Považay, A. Baltuška, and A. Pugžlys, Influence of 2.09-μm pulse duration on through-silicon laser ablation of thin metal coatings, Opt. Laser Technol., **133**, 106535, (2021).

[20] H. Zheng, Z. Bai, X. Hao, J. Ding, Y. Qi, B. Yan, Y. Wang, and Z. Lu, Investigation of the pulse characteristics of an injection seeded diamond Raman amplifier, Appl. Phys. Lett., **125**(13), (2024).

[21] F. Möller, T. Lühder, B. Yildiz, T. Walbaum, and T. Schreiber, Spectral beam combining of kW-class thulium-doped fiber lasers, Proc. SPIE 12865, Fiber Lasers XXI: Technology and Systems, 128650S (2024).

[22] C. Gaida, M. Gebhardt, T. Heuermann, F. Stutzki, C. Jauregui, and J. Limpert, Ultrafast thulium fiber laser system emitting more than 1 kW of average power, Opt. Lett., **43**(23), 5853, (2018).

[23] D. C. Kirsch, S. Chen, R. Sidharthan, Y. Chen, S. Yoo, and M. Chernysheva, Short-wave IR ultrafast fiber laser systems: Current challenges and prospective applications, J. Appl. Phys., **128**(18), (2020).

[24] P. Malevich, G. Andriukaitis, T. Flory, A. Verhoef, A. Fernandez, S. Ališauskas, A. Baltuška, L. Tan, C. Chua, P. Phua, High-Repetition-Rate Multi-Millijoule Femtosecond 2.1-µm Ho:YAG Laser, Proc. Advanced Solid-State Laser Congress, AF1A.4., (2013).

[25] M. Bock, D. Ueberschaer, M. Mero, T. Nagy, and U. Griebner, 2.05 µm CPA delivering 75 mJ pulses with 2.2 ps duration at a 1 kHz repetition rate, Opt. Express, **33**(8), 17245, (2025).

[26] J. I. Mackenzie, W. O. S. Bailey, J. W. Kim, L. Pearson, D. Y. Shen, Y. Yang, and W. A. Clakson, Tm:fiber laser in-band pumping a cryogenically-cooled Ho:YAG laser, Proc. of SPIE, **7193**, 71931H, (2009).

[27] J. Zhang, F. Schulze, K. F. Mak, V. Pervak, D. Bauer, D. Sutter, and O. Pronin, High-Power, High-Efficiency Tm:YAG and Ho:YAG Thin-Disk Lasers, Laser Photon. Rev., **12**(3), (2018).

[28] C. W. Rudy, M. J. F. Digonnet, and R. L. Byer, Advances in 2-µm Tm-doped mode-locked fiber lasers, Opt. Fiber Technol., **20**(6), 642–649, (2014).

[29] F. Stutzki, C. Gaida, M. Gebhardt, F. Jansen, A. Wienke, U. Zeitner, F. Fuchs, C. Jauregui, D. Wandt, D. Kracht, J. Limpert, and A. Tünnermann, 152 W average power Tm-doped fiber CPA system, Opt. Lett., **39**(16), 4671, (2014).

[30] P. Malevich, G. Andriukaitis, T. Flöry, A. J. Verhoef, A. Fernández, S. Ališauskas, A. Pugžlys, A. Baltuška, L. H. Tan, C. F. Chua, and P. B. Phua, High energy and average power femtosecond laser for driving mid-infrared optical parametric amplifiers, Opt. Lett., **38**(15), 2746, (2013).

[31] M. Hemmer, D. Sánchez, M. Jelínek, Vadim Smirnov, H. Jelinkova, V. Kubeček, and J. Bieger, 2-µm wavelength, high-energy Ho:YLF chirped-pulse amplifier for mid-infrared OPCPA, Opt. Lett., **40**(4), 451, (2015).

[32] S. Tomilov, M. Redkin, Y. Wang, A. Suzuki, M. Hoffmann, and C. J. Saraceno, Energy scaling of Kerr-lens modelocked Ho:YAG thin-disk oscillators to the microjoule level, Opt. Express, **33**(12), 25932, (2025).

[33] S. A. Rezvani and T. Fuji, Millijoule 265 fs Tm:YAP regenerative amplifier for driving ultrabroad band collinear mid-infrared optical parametric amplifiers, Opt. Express, **30**(5), 7332, (2022).

[34] A. Tyazhev, J. E. Bae, M. Gaulke, P. Loiko, J. Heidrich, M. Golling, S. Idlahcen, L. Guillemot, T. Godin, P. Camy, U. Keller, and A. Hideur, Upconversion-pumped femtosecond thulium laser at 2309 nm mode-locked by a GaSb-based SESAM, Opt. Express, **32**(9), 15093, (2024).

[35] X. Hu, K. F. Mak, J. Zhang, Z. Wei, and F. Krausz, Ultrafast lasers for attosecond science, Light Sci. Appl., **15**(24), (2026).

[36] Z. Wang, T. Heuermann, M. Gebhardt, M. Lenski, P. Gierschke, R. Klas, J. Rothhardt, C. Jauregui, and J. Limpert, Nonlinear pulse compression to sub-two-cycle, 1.3 mJ pulses at 1.9 μm wavelength with 132 W average power, Opt. Lett., **48**(10), 2647, (2023).

[37] A. Dubietis and A. Matijošius, Table-top optical parametric chirped pulse amplifiers: past and present, Opto-Electron. Adv., **6**, 220046, (2023).

[38] H. Fattahi, N. Karpowicz, T. Metzger, Z. Major, and F. Krausz, Third-generation femtosecond technology, Optica, **1**(1), 45-63, (2014).

[39] R. Riedel, M. Schulz, M. J. Prandolini, A. Hage, H. Hoppner, T. Gottschall, J. Limpert, M. Drescher, and F. Tavella, Long-term stabilization of high power optical parametric chirped-pulse amplifiers, Opt. Express, **21**(23), 28987, (2013).

[40] E. Smith and G. Dent, *Modern Raman spectroscopy: a practical approach*. (John Wiley and Sons, Ltd, 2005).

[41] D. Von Der Linde, M. Maier, and W. Kaiser, Quantitative Investigations of the Stimulated Raman Effect Using Subnanosecond Light Pulses, Phys. Rev., **178**(1), 11-17, (1969).

[42] J. Li, H. Li, and Z. Wang, Application of hollow-core photonic crystal fibers in gas Raman lasers operating at 1.7 μm, Crystals, **11**(2), (2021).

[43] P. Mackonis, A. Petrulenas, A. M. Rodin, V. Girdauskas, and A. Michailovas, Two-stage transient stimulated Raman chirped-pulse amplification in $KGd(WO_4)_2$ with compression to 145 fs, Opt. Lett., **45**(24), 6627, (2020).

[44] C. V Raman and K. S. Krishnan, A new type of secondary radiation, Nature, **121**, 501-502, (1928).

[45] E. J. Woodbury and W. K. Ng, Ruby Laser Operation in the Near IR, Proc. Inst. Radio Eng., **50**(11), 2367, (1962).

[46] R. W. Hellwarth, Theory of Stimulated Raman Scattering, Phys. Rev., **130**(5), 1850-1852, (1963).

[47] Audrius Dubietis, *Netiesinė optika*, (Vilniaus Universitetas, 2011).

[48] D. C. Hanna, D. J. Pointer, and D. J. Pratt, Stimulated Raman scattering of picosecond light pulses in hydrogen, deuterium, and methane, IEEE J. Quantum Electron., **22**(2), 332-336, (1986).

[49] N. Zhavoronkov, F. Noack, V. Petrov, V. P. Kalosha, and J. Herrmann, Chirped pulse stimulated Raman scattering in barium nitrate with subsequent recompression, Opt. Lett., **26**(1), (2001).

[50] G. Hilfer and C. R. Menyuk, Stimulated Raman scattering in the transient limit, J. Opt. Soc. Am. B, **7**(5), (1990).

[51] Y. Uesugi, Y. Mizutani, S. G. Kruglik, A. G. Shvedko, V. A. Orlovich, and T. Kitagawa, Characterization of stimulated Raman scattering of hydrogen and methane gases as a light source for picosecond time-resolved Raman spectroscopy, J. Raman Spectrosc., **31**, 339-348, (2000).

[52] C. Jordan, K. A. Stankov, G. Marowsky, and E. J. Canto-Said, Efficient compression of femtosecond pulses by stimulated Raman scattering, Appl. Phys. B, **59**, 471-473, (1994).

[53] A. Gladyshev, Y. Yatsenko, A. Kolyadin, V. Kompanets, and I. Bufetov, Mid-infrared 10-μJ-level sub-picosecond pulse generation via stimulated Raman scattering in a gas-filled revolver fiber, Opt. Mater. Express, **10**(12), 3081, (2020).

[54] A. I. Vodchits, A. G. Shvedko, V. A. Orlovich, V. P. Kozich, and W. Werncke, Stimulated Raman amplification of ultrashort seed pulses in compressed methane, J. Opt. Soc. Am. B, **22**(2), 453-458, (2005).

[55] F. B. Grigsby, P. Dong, and M. C. Downer, Chirped-pulse Raman amplification for two-color, high-intensity laser experiments, J. Opt. Soc. Am. B, 25(3), 346-350, (2008).

[56] V. Krylov, A. Rebane, D. Erni, O. Ollikainen, and U. Wild, Stimulated Raman amplification of femtosecond pulses in hydrogen gas, Opt. Lett. **21**(24) (1996).

[57] O. V Buganov, A. S. Grabtchikov, Y. I. Malakhov, Y. M. Popov, V. A. Orlovich, and S. A. Tikhomirov, Features of Raman amplification in KGW and barium nitrate crystals at excitation by femtosecond pulses, Laser Phys. Lett., **9**(11), 786-789, (2012).

[58] A. Petrulėnas, P. Mackonis, A. Černeckytė, and A. M. Rodin, Amplification of Supercontinuum Seed Pulses at ~1078–1355 nm by Cascade Rotational SRS in Compressed Hydrogen, Appl. Sci., **13**(24), (2023).

[59] P. Mackonis and A. M. Rodin, Laser with 1.2 ps, 20 mJ pulses at 100 Hz based on CPA with a low doping level Yb:YAG rods for seeding and pumping of OPCPA, Opt. Express, **28**(2), 1261, (2020).

[60] D. J. Kane and R. Trebino, Characterization of Arbitrary Femtosecond Pulses Using Frequency-Resolved Optical Gating, IEEE J. Quantum Electron., **29**(2), 571-579, (1993).

Santrauka

Augustė Grigaravičienė

ULTRATRUMPŲJŲ IMPULSŲ GENERACIJOS TYRIMAS TRUMPABANGĖJE INFRARAUDONOJOJE SPEKTRO SRITYJE TAIKANT PRIVERSTINĘ RAMANO SKLAIDĄ

Didelės energijos ultratrumpųjų impulsų generacija trumpabangėje infraraudonojoje (SWIR) spektro srityje šiuo metu yra viena iš vystomų lazerių fizikos sričių, apimanti taikymus nuo puslaidininkių apdirbimo iki aukštesniųjų harmonikų generacijos. Visgi pasiekti SWIR sritį vis dar yra sudėtingas, neefektyvus ir daug išteklių reikalaujantis procesas. Skaiduliniai tuliu legiruoti lazeriai dažnai pasižymi ribota smailine galia dėl parazitinių netiesinių reiškinių, o kieto kūno holmiu legiruoti lazeriai reikalauja nestandartinio bangos ilgio kaupinimo šaltinių bei brangaus kriogeninio aušinimo. Gerai išvystytoms šiuolaikinėms optinių parametrinių čirpuotų impulsų stiprinimo (OPCPA) sistemoms būdingos sudėtingos daugiapakopės konfigūracijos, griežtas fazinis sinchronizmas ir didelių matmenų išoriniai impulsų spaustuvai, norint pasiekti kelių optinių ciklų trukmę.

Šiame magistro darbe tiriama nenuostovioji priverstinė Ramano sklaida (SRS) suslėgtų vandenilio dujų kiuvetėje. Vandenilis pasižymi dideliu vibraciniu Ramano poslinkiu (4155 cm^{-1}), kuris leidžia tiesiogiai generuoti SWIR srities ~1,8 μm bangos ilgio Stokso impulsus kaupinimui naudojant standartinį 1 μm lazerį. Eksperimentinėje schemoje naudoti 1,3 ps trukmės, 1030 nm centrinio bangos ilgio kaupinimo impulsai ir superkontinuumo užkratas, kuris išfiltruojamas taip, kad centrinis bangos ilgis atitiktų vibracinio Stokso spinduliuotės centrinį bangos ilgį.

Pasiektas rekordiškai aukštas SRS keitimo efektyvumas lygus 30,2% (atitinkantis 52,8% kvantinį efektyvumą), Stokso impulsų energija siekė 0,36 mJ. Kitas svarbus šio darbo rezultatas – nustatyta laikinio vėlinimo tarp kaupinimo ir užkrato impulsų svarba. Nors impulsams persiklojant pasiektas aukštas efektyvumas ir gauti 575 fs trukmės Stokso impulsai, laikinis vėlinimas leido pasiekti devynis kartus didesnį impulsų spektrinį plitimą, suformuojant Stokso impulsus, kurių trukmė 146 fs, o keitimo efektyvumas lygus 15,7%. Stokso impulso smailinė galia siekė 1,91 GW ir 1,55 kartų viršijo kaupinimo impulso smailinę galią.

Ateities tyrimai bus orientuoti į sistemos impulsų pasikartojimo dažnio didinimą, taip pritaikant šią sistemą lazeriniam apdirbimui. Tam bus būtina spręsti šiluminės akumuliacijos vandenilio terpėje problemas. Be to, panaudojus papildomą netiesinės spūdos pakopą (pvz., argono dujų kiuvetę) galima formuoti didelės energijos kelių optinių ciklų trukmės impulsus SWIR srityje.

Summary

Augustė Grigaravičienė

INVESTIGATION OF ULTRASHORT PULSE GENERATION IN THE SHORT-WAVE INFRARED SPECTRAL REGION USING STIMULATED RAMAN SCATTERING

The goal of creating high-energy, ultrashort pulse sources in the short-wave infrared (SWIR) spectral region has become a major area of interest due to their potential applications ranging from semiconductor manufacturing to high-harmonic generation. There are several technologies that have been used to generate radiation in the SWIR region including thulium and holmium doped lasers and optical parametric chirped pulse amplifiers (OPCPAs). However, these technologies also present some limitations. For example, fiber-based thulium architectures are often limited in peak power by parasitic nonlinearities. Additionally, bulk holmium-based systems typically require non-standard pumping and expensive cryogenic cooling. Lastly, state-of-the-art OPCPAs necessitate complex multi-stage configurations, strict phase-matching conditions and bulky external compressor stages to produce few-optical cycle durations.

In this master's thesis we propose a scalable alternative by investigating transient stimulated Raman scattering (SRS) in a high-pressure hydrogen gas cell. The hydrogen was chosen because of its relatively large vibrational Raman shift of 4155 cm^{-1}. Therefore, standard 1 μm Yb-based laser radiation can be directly converted into the 1.8 μm SWIR region in a single Raman conversion step. The experimental setup employed 1.3 ps pump pulses centered at 1030 nm wavelength and a supercontinuum seed filtered via an acousto-optic programmable dispersive filter (AOPDF).

Key experimental results include a record-high energy conversion efficiency of 30.2% (corresponding to a quantum efficiency of 52.8%), which resulted in Stokes pulse energies of up to 0.36 mJ. Another finding of this work is the significant role of the temporal delay between the pump and seed pulses. Specifically, when no temporal delay existed between the pulses, near-transform-limited Stokes pulses of 575 fs were generated. However, when a temporal delay was introduced, it enabled a nine-fold temporal self-compression, resulting in Stokes pulses as short as 146 fs. As a result, the peak power of the Stokes pulse reached 1.91 GW, whereas the peak power of the pump laser was 1.23 GW.

The future research will focus on increasing the pulse repetition rate of our system to levels suitable for practical use in laser processing. In addition to addressing thermal accumulation and density perturbations in the hydrogen, we plan to implement nonlinear compression stage using an argon filled gas cell that will broaden the spectrum of the Stokes pulse via self-phase modulation and thus enable us to obtain high energy pulses in the SWIR range with durations approaching the few-cycle regime.